Calculation and Accuracy of ERBE Scanner Measurement Locations

Lawrence H. Hoffman,
William L. Weaver,
and James F. Kibler

NASA

Calculation and Accuracy of ERBE Scanner Measurement Locations

Lawrence H. Hoffman,
William L. Weaver,
and James F. Kibler

Langley Research Center
Hampton, Virginia

Summary

The Earth Radiation Budget Experiment (ERBE) uses scanning radiometers to measure shortwave and longwave components of the Earth's radiation field at about 40 km resolution. It is essential that these measurements be accurately located at the top of the Earth's atmosphere so they can be properly interpreted by users of the data. Before the launch of the ERBE instrument sets, a substantial emphasis was placed on understanding all factors which influence the determination of measurement locations and properly modelling those factors in the data processing system. After the launch of ERBE instruments on the Earth Radiation Budget Satellite and NOAA 9 spacecraft in 1984, a coastline detection method was developed to assess the accuracy of the algorithms and data used in the location calculations. Using inflight scanner data and the coastline detection technique, the measurement location errors are found to be smaller than the resolution of the scanner instruments. This accuracy is well within the required location knowledge for useful science analyses.

Introduction

The Earth Radiation Budget Experiment (ERBE) is a three-satellite mission designed to measure components of the Earth's radiation field. Three satellites, Earth Radiation Budget Satellite (ERBS), NOAA 9, and NOAA 10, are now in orbit. Each satellite carries two ERBE instruments, the scanner and the nonscanner. The scanner has three Earth viewing radiometers, which make a total radiation measurement and broadband radiance measurements in the shortwave and longwave parts of the energy spectrum. The three scanner channels are coaligned and nominally scan the Earth every 4 seconds from horizon to horizon in a plane normal to the orbit plane. The nonscanner has four Earth viewing channels and a solar monitor channel. Two of the Earth viewing channels measure the total radiation and two measure the shortwave component. A single nonscanner measurement covers a large area of the Earth, and the scanner has a field of view (FOV) of about 40 km in diameter at nadir.

Two different spacecraft are used to carry the ERBE instruments, and each is operated by a separate agency. The National Aeronautics and Space Administration (NASA) Goddard Space Flight Center (GSFC) operates the ERBS, which was launched on the Shuttle Challenger in October 1984. The Earth Radiation Budget Satellite is in a near-circular 600-km orbit with an inclination of 57°. The National Oceanographic and Atmospheric Adminis-tration (NOAA) controls the NOAA 9 operational weather-monitoring satellite, which was launched into a polar orbit in December 1984. The NOAA 9 satellite is in a sun-synchronous near-circular 856-km orbit. Langley Research Center (LaRC) is responsible for the ERBE instrument development, science management, and data processing.

The development of the experiment and the sensors, as well as the stringent accuracy requirements of the mission, are described in reference 1. One element of the overall measurement accuracy is the requirement to locate the center of the FOV of each measurement. Both the surface characteristics at the measurement location and the satellite-Earth-Sun geometry are important factors used in the interpretation of the radiometric channels. Thus, it is essential that the measurement be accurately located with respect to the surface of the Earth. This task is complicated by the fact that, since there is no imaging system onboard the ERBS spacecraft, landmark identification is difficult.

The ERBE project personnel began to analyze the factors affecting the accuracy several years before launch of the satellites. Beginning with the source of the data, LaRC documented agreements with GSFC and NOAA which define the data interfaces to the LaRC processing system. The documents specify a consistent set of orbital position data for each satellite and determine the coordinate systems used for measurements made from each spacecraft. The agreements also specify the format, content, and interpretation of the spacecraft attitude data derived from the onboard attitude determination and control systems. The orbital position data and spacecraft attitude data permit the calculation of the location and orientation of the satellite, factors essential to the accurate determination of the measurement location. Since the coordinate systems used to derive the various data types are different, position and attitude data must be transformed to a common coordinate system for interpretation and subsequent calculations. This step is the first key factor in understanding the accuracy of the measurement locations.

Another accuracy factor involves the alignment of the radiometric instruments themselves with the satellite structure. Langley Research Center engineers monitored the instrument development contract with the prime contractor and measured the alignment of the instrument coordinate system with each spacecraft. These alignments are included in the measurement location calculations.

Many of the remaining steps in calculating the measurement location require geometry transformations or modelling of the Earth's surface

to describe intersection points. All these steps were carefully derived and checked prior to launch.

The purpose of this paper is to describe each step in the calculation of ERBE measurement locations and to evaluate the accuracy of the calculations. Since the scanner instrument requires much more stringent pointing accuracy than the nonscanner instrument, the discussion is limited to the scanner instrument. The same concepts are used in locating the nonscanner measurements. The motivation for the analysis is to verify that the pointing algorithms are correct and to confirm the validity of the radiometric data location for science investigations.

Symbols

A,B,C,D,E,F,G	rotation matrices
h	height of top of atmosphere above Earth ellipsoid, km
$\vec{P}$	vector from center of Earth to spacecraft
R	Earth radius, km
V	velocity, m/sec
$\vec{V}$	vector from spacecraft to intersection with Earth
$\hat{V}$	unit pointing vector
X, Y, Z	Cartesian axes
α	instrument azimuth angle, deg
β	instrument elevation angle, deg
Δ	difference between geodetic and geocentric latitude, deg
ϵ	error, deg
η	spacecraft heading angle, deg
θ	pitch angle, deg
Λ	longitude, deg
ν	inertial longitude of Greenwich meridian, deg
Φ	latitude, deg
ϕ	roll angle, deg
ψ	yaw angle, deg

Subscripts:

a	along track
C	geocentric
c	cross track
D	detector
E	ERBS
e	equatorial
F	Earth fixed
G	geodetic
H	local horizon
I	inertial
N	NOAA
P	pedestal
p	polar
α	azimuth
β	elevation

Abbreviations:

ADACS	Attitude Determination and Control System
ERBE	Earth Radiation Budget Experiment
ERBS	Earth Radiation Budget Satellite
FOV	field of view
GSFC	Goddard Space Flight Center
LaRC	Langley Research Center
NASA	National Aeronautics and Space Administration
NESDIS	National Environmental Satellite and Data Information Service
NOAA	National Oceanographic and Atmospheric Admininstration
TOA	top of atmosphere

Calculation of Scanner Measurement Location

The determination of the scanner-measurement location can be separated into two major steps. In the first step, the unit pointing vector of the optical axis of the detectors is calculated in a local-horizon system located at the spacecraft. In the second step, the detector pointing vector is transformed from the local-horizon system to an Earth fixed coordinate system in which the measurement location is determined on a surface 30 km above the Earth. This surface is called the top of atmosphere (TOA) and has been selected as a reference surface for outgoing radiation.

Calculation of Detector Pointing Vectors in Local-Horizon System

In this first major step in determining the scanner measurement location, a unit vector which is aligned with the scanner optical axis is computed in a local-horizon coordinate system. This section describes the different coordinate transformations that relate the components of the detector pointing vector in the detector coordinates to its components in spacecraft coordinates. The discussion includes consideration of detector misalignments, a description of the telemetry data, and the computations required to determine the pointing vector in spacecraft coordinates. This description is followed by a discussion of the transformation of the pointing vector, through the use of the spacecraft attitude data, to the local-horizon coordinate system of the particular spacecraft. Finally, the pointing vector is transformed to a local-horizon system that is common to both the ERBS and NOAA spacecraft.

Detector-to-Spacecraft Coordinate Transformations

Figure 1 illustrates the coordinate systems which relate the position and orientation of the scanner detectors to the coordinate system of the instrument pedestal. The pedestal physically attaches the instrument system to the spacecraft, and the relationship between the coordinate system of the pedestal and those of the TIROS N (NOAA) and ERBS spacecraft is illustrated in figure 2. Only the orientation of these coordinate systems relative to each other is important to the measurement location calculations, and a unit vector describing the direction of the scanner detectors is assumed to have its origin at the focal point of the detectors.

The three scanner detectors shown at the bottom of figure 1 have 2 degrees of freedom relative to the pedestal. The azimuth assembly (the entire system below the pedestal) can rotate (change azimuth) about the X_P-axis, so that the instrument can be pointed during solar calibration and so that measurements can be made while scanning at azimuth positions from $0°$ to $180°$. The azimuth assembly is shown at the zero-azimuth ($\alpha = 0°$) position, and a positive rotation (azimuth increasing) produces a positive rotation vector along the X_P-axis. The elevation beam on which the detectors are mounted (small substructure on azimuth assembly) can rotate (change elevation or scan) about the Y_β-axis. Elevation, or scan angle, is measured from the Y_α-Z_α plane, and a positive rotation produces a positive rotation vector along the Y_β-axis. The detectors shown in figure 1 are at an elevation scan angle of $90°$.

To determine the complete matrix which transforms the detector pointing vectors into spacecraft coordinates, the matrix which transforms a pointing vector in one of the spacecraft coordinate systems to its components in the detector coordinate system should be defined first. The complete series of rotations which effect this vector transformation is given below:

$$\begin{bmatrix} X_D \\ Y_D \\ Z_D \end{bmatrix} = \mathbf{DCBA}_E \begin{bmatrix} X_E \\ Y_E \\ Z_E \end{bmatrix} \qquad (1)$$

$$\begin{bmatrix} X_D \\ Y_D \\ Z_D \end{bmatrix} = \mathbf{DCBA}_N \begin{bmatrix} X_N \\ Y_N \\ Z_N \end{bmatrix} \qquad (2)$$

where the pedestal-to-spacecraft alignment for each spacecraft is

$$\mathbf{A}_E = \begin{bmatrix} 0 & 0 & 1 \\ 1 & 0 & 0 \\ 0 & 1 & 0 \end{bmatrix}$$

ERBS

$$\mathbf{A}_N = \begin{bmatrix} 1 & 0 & 0 \\ 0 & -1 & 0 \\ 0 & 0 & -1 \end{bmatrix}$$

NOAA

3

and where the azimuth, elevation, and detector rotations for the ERBS and NOAA spacecraft are

$$\mathbf{B} = \begin{bmatrix} 1 & 0 & 0 \\ 0 & \cos\alpha & \sin\alpha \\ 0 & -\sin\alpha & \cos\alpha \end{bmatrix}$$

$$\mathbf{C} = \begin{bmatrix} \cos\beta & 0 & -\sin\beta \\ 0 & 1 & 0 \\ \sin\beta & 0 & \cos\beta \end{bmatrix}$$

$$\mathbf{D} = \begin{bmatrix} 0 & 0 & 1 \\ 0 & 1 & 0 \\ -1 & 0 & 0 \end{bmatrix}$$

The matrix $\mathbf{A}$ is the transformation from the spacecraft coordinate system to the instrument pedestal coordinate system. The alignment of these systems is shown for the ERBS and NOAA spacecraft in figure 2. The matrix $\mathbf{B}$ is the transformation from the pedestal coordinate system to a new coordinate system $(X_\alpha, Y_\alpha, Z_\alpha)$, which results when the instrument azimuth axes are rotated away from the pedestal axes about the X_P-axis. (See fig. 1.) This azimuth rotation is positive when the rotation is positive about the X_P-axis. The matrix $\mathbf{C}$ is the transformation from the azimuth coordinate system to the coordinate system $(X_\beta, Y_\beta, Z_\beta)$, which results when the instrument elevation beam is rotated away from the azimuth coordinate system about the Y_β-axis. This elevation rotation is positive when the rotation vector is positive along the Y_β-axis. In this new coordinate system, the detector scan head is aligned approximately with the X_P-axis when the elevation or scan angle is zero, whereas the elevation angle output of the instrument assumes that the detector scan head lies approximately in the $Y_\beta - Z_\beta$ plane when the elevation angle is $0°$. A final transformation, matrix $\mathbf{D}$, transforms from the elevation coordinate system to the detector coordinate system by a $-90°$ rotation about Y_β to give the vector components in the detector coordinate system (X_D, Y_D, Z_D).

Finally, to transform the pointing vectors from the detector coordinate system to one of the spacecraft coordinate systems, the transpose of the matrices in equations (1) and (2) is used. The complete transformations of the vectors for the two spacecraft can thus be written as follows:

$$\begin{bmatrix} X_E \\ Y_E \\ Z_E \end{bmatrix} = \begin{bmatrix} -\cos\beta\sin\alpha & \cos\alpha & -\sin\beta\sin\alpha \\ \cos\beta\cos\alpha & \sin\alpha & \sin\beta\cos\alpha \\ \sin\beta & 0 & -\cos\beta \end{bmatrix} \begin{bmatrix} X_D \\ Y_D \\ Z_D \end{bmatrix} \quad (3)$$

$$\begin{bmatrix} X_N \\ Y_N \\ Z_N \end{bmatrix} = \begin{bmatrix} \sin\beta & 0 & -\cos\beta \\ \cos\beta\sin\alpha & -\cos\alpha & \sin\beta\sin\alpha \\ -\cos\beta\cos\alpha & -\sin\alpha & -\sin\beta\cos\alpha \end{bmatrix} \begin{bmatrix} X_D \\ Y_D \\ Z_D \end{bmatrix} \quad (4)$$

If there are no misalignments of the detectors with respect to the axes of the spacecraft on which they are mounted, the components of the pointing vector which is aligned with the detector optical axis, or initial pointing vector, are given by

$$X_D = 1$$
$$Y_D = 0$$
$$Z_D = 0$$

Detector misalignments. This section describes the procedures that were followed during construction of the ERBS instrument to minimize and record detector misalignment, and the methods by which these measurements were incorporated into the algorithms used to compute the pointing vectors. These procedures were carried through the several contractors involved in the design and construction of the instruments and the spacecraft, and were carefully monitored by LaRC engineering personnel at all stages. Angular alignment data and analysis for the instrument on NOAA 9 have not been reduced to values which can be used to compute the initial pointing error. Therefore, no detector misalignments have been assumed in computing the in-flight detector pointing vectors for NOAA 9.

Preliminary alignment measurements for the instrument on the ERBS spacecraft have been used to compute the initial pointing vector of the detectors. The components of that initial pointing vector are

$$X_D = 0.999999182$$
$$Y_D = -0.001197480$$
$$Z_D = -0.001005180$$

More recent values of scanner detector angle misalignments for the instrument on the ERBS spacecraft give an initial detector pointing vector with the following components:

$$X_D = 0.999999654$$
$$Y_D = -0.000824330$$
$$Z_D = 0.001221080$$

If the revised alignment data were assumed to be correct, the pointing vectors computed using the preliminary alignment data result in a 1.2-km scanner measurement location error at nadir in the direction of the scan motion. This error, which is a bias in the instrument and spacecraft coordinate systems, changes direction in the local-horizon system when the ERBS spacecraft yaws 180° approximately every 36 days. The resulting along-track error using the preliminary alignment data is about 200 m down-range when the spacecraft is flying with the X-axis forward and 200 m uprange when the X-axis is rearward. Although there are small differences between the preliminary and revised values, the preliminary data have been used in all in-flight computations of ERBS scanner pointing vectors.

Overview of telemetry data. The telemetry data from the ERBS and NOAA spacecraft are acquired and processed initially for LaRC by the Information Processing Divisions at GSFC and NOAA/NESDIS, respectively. Twenty-four-hour data sets are formatted into logical data records, each containing 16 seconds of data and an associated universal time. The various types of data are sampled at different rates, and the universal time of any data word in a record is obtained by adding a specified time offset to the record time. The time offset for any data word in a record is a constant for all records for each spacecraft.

The scanner instrument has a 4-second scan period, and each 16-second record contains 4 complete cycles of instrument radiometric and housekeeping data. The data in a 4-second cycle consist of 74 sets of measurements, and each set consists of one measurement from each of the three radiometric channels and a corresponding value for the detector scan head elevation angle. The instrument housekeeping data include, besides temperature and voltage measurements, detector azimuth and elevation angles and instrument command and status information. Spacecraft housekeeping data include spacecraft attitude data and spacecraft operational status information. The following sections describe how the raw instrument data and spacecraft housekeeping data are processed to determine the detector pointing vectors for the scanner radiometric measurements.

Azimuth-angle data. In the normal Earth viewing data-acquisition mode, the scanner azimuth is set for crosstrack scanning (in a plane normal to the orbit plane). The azimuth position is 180° for the ERBS spacecraft and 0° for the NOAA spacecraft. Periodically, the azimuth assembly is rotated to obtain solar calibration data, and it is occasionally rotated to the 90° azimuth position to obtain along-track measurements.

Four raw values (one for each scan cycle) of instrument azimuth position are contained in each 16-second telemetry data record. Instrument command and status data are checked to deduce the operational mode of the instrument and to determine whether a mode-change command has been issued for the record or whether the azimuth assembly is in motion. If the operational mode is explicitly determined from the data, if no new operational command has been issued for the record, and if the azimuth assembly is not in motion, the first raw value of azimuth position in the record is decoded and converted to an azimuth angle. If the converted azimuth value is an acceptable azimuth angle and passes all edit tests, it is used in the computation of all space scanner detector pointing vectors for the record. In all other cases, no valid detector pointing vectors are computed for the record.

Elevation- or scan-angle data. The three radiometric measurements and the associated elevation angle in a data set are all sampled within a few microseconds of each other. Sixty-two of the 74 measurement sets in a 4-second scan cycle are sampled every $33\frac{1}{3}$ milliseconds. For the normal Earth scan mode, these 62 measurements are made while the detector is scanning the Earth from horizon to horizon. Even though each measurement set is sampled at a constant time offset relative to the record time, and even though the Earth viewing measurement sets are equally spaced in time, the elevation angle associated with a specific measurement set in a scan cycle differs from scan to scan within a record and from record to record. Because of this variation from scan to scan, a new detector pointing vector is computed for every measurement set.

A detector pointing vector is computed only if the corresponding elevation angle is valid. The validation of the elevation-angle data involves checking the instrument command and status words and editing the converted elevation angle. The conversion of a raw elevation value is dependent on the specific scan mode of the instrument. If the scan mode cannot be determined from the command and status words, or is changing during a record, no values of elevation angle are considered valid for the record; thus, no detector pointing vectors are computed. If the scanner is in the stowed mode, Earth viewing data are not available and no elevation angles are computed. Finally, before a converted elevation angle is used in computing a pointing vector, its value is tested and must be within specified bounds.

Adjustment to detector elevation angle before computing pointing vector. Before the validated scan elevation angle can be used in the detector

pointing vector calculations, it is adjusted to account for scanner response time. In ERBE instrument studies at LaRC, it was concluded that the ERBE scanner radiometric detectors have a response time of 46 milliseconds. This response time is greater than the $33\frac{1}{3}$-millisecond interval between consecutive radiometric measurements during the Earth viewing portion of a scan cycle. To account for this time lag, the scanner measurement locations are computed to match a set of radiometric detector outputs with the measurement locations that the detectors were viewing 46 milliseconds earlier.

The four dynamic factors which affect the scanner Earth measurement locations are as follows: (1) rotational motion of the Earth, (2) spacecraft orbit motion, (3) spacecraft attitude motion, and (4) scan head elevation motion. At the equator, the Earth's motion in 46 milliseconds is less than 25 m. The along-track spacecraft distance traveled in 46 milliseconds is only 317 m for ERBS and 300 m for the NOAA-9 spacecraft. Changes in the location at nadir in 46 milliseconds as the result of attitude motion are normally less than 25 m and do not exceed 50 m. The ERBE scan head elevation beam rotates at a rate of 66.7° per second during the Earth viewing portion of the scan cycle and thus rotates 3.066° in 46 milliseconds. Earth distances measured at nadir due to this angular change are 32 km and 46 km for the ERBS and NOAA-9 spacecraft, respectively. Because the combined changes in measurement location due to Earth rotation (0.02 km), spacecraft orbit motion (0.3 km), and attitude motion (0.05 km) are very small in 46 milliseconds compared with the change due to elevation beam rotation (46 km), only the scan motion is considered in correcting the measurement locations. The actual adjustment in measurement location is made by computing the detector pointing vector in the spacecraft coordinate system using an effective detector elevation angle 3.066° less than the measured elevation angle. The most noticeable effect of this adjustment is that the measurements are shifted toward the side where the scan begins.

Transformation From Spacecraft Coordinates to Local-Horizon Coordinates

This section describes how the detector pointing vectors determined in a spacecraft coordinate system are transformed into a common local-horizon system centered on the spacecraft. This local-horizon system is illustrated in figure 3, which also shows the relationship between the X-, Y-, and Z-axes of the system and the physical quantities which define the system. The X-axis is down and normal to the local-horizon plane, the Y-axis lies along the negative component of the spacecraft velocity vector in the local-

horizon tangent plane, and the Z-axis is parallel to the orbit angular-momentum vector. A description of the orbit ephemeris data used to compute the position of the origin and the orientation of this coordinate system is given in the next section.

The first step in transforming the detector pointing vectors into local-horizon coordinates is to compute the pointing vectors in the local-horizon system for the specific spacecraft. The components of the detector pointing vectors in a spacecraft coordinate system and its components in the spacecraft-dependent local-horizon system are related through the spacecraft orientation or attitude angles. (See fig. 4.) This relationship is different for the two spacecraft, both in the designation of the axes and in the manner and order of the rotations of the axes.

The transformation of the detector pointing vectors to the ERBS local-horizon axis system, given its components in the ERBS spacecraft system, is given as follows:

$$\begin{bmatrix} X_{H,E} \\ Y_{H,E} \\ Z_{H,E} \end{bmatrix} = \mathbf{G}_E \mathbf{F}_E \mathbf{E}_E \begin{bmatrix} X_E \\ Y_E \\ Z_E \end{bmatrix} \tag{5}$$

where

$$\mathbf{E}_E = \begin{bmatrix} \cos\theta & 0 & \sin\theta \\ 0 & 1 & 0 \\ -\sin\theta & 0 & \cos\theta \end{bmatrix}$$

$$\mathbf{F}_E = \begin{bmatrix} 1 & 0 & 0 \\ 0 & \cos\phi & -\sin\phi \\ 0 & \sin\phi & \cos\phi \end{bmatrix}$$

$$\mathbf{G}_E = \begin{bmatrix} \cos\psi & -\sin\psi & 0 \\ \sin\psi & \cos\psi & 0 \\ 0 & 0 & 1 \end{bmatrix}$$

The transformation of the detector pointing vectors to the NOAA local-horizon system, given its components in the NOAA spacecraft system, is given as follows:

$$\begin{bmatrix} X_{H,N} \\ Y_{H,N} \\ Z_{H,N} \end{bmatrix} = \mathbf{G}_N \mathbf{F}_N \mathbf{E}_N \begin{bmatrix} X_N \\ Y_N \\ Z_N \end{bmatrix} \tag{6}$$

where

$$\mathbf{E}_N = \begin{bmatrix} \cos\theta & \sin\theta & 0 \\ -\sin\theta & \cos\theta & 0 \\ 0 & 0 & 1 \end{bmatrix}$$

$$\mathbf{F}_N = \begin{bmatrix} \cos\phi & 0 & -\sin\phi \\ 0 & 1 & 0 \\ \sin\phi & 0 & \cos\phi \end{bmatrix}$$

$$\mathbf{G}_N = \begin{bmatrix} 1 & 0 & 0 \\ 0 & \cos\psi & \sin\psi \\ 0 & -\sin\psi & \cos\psi \end{bmatrix}$$

Sixteen sets of attitude angles (roll, pitch, and yaw) are contained in a telemetry record (one set per second). Since the attitude-angle sampling rate is much slower than the radiometric sampling rate, the pointing vectors for each second of radiometric data are computed using the set of attitude angles whose time most closely matches the average time of the 1-second group of radiometric data. Operations status data indicating the operational modes of the spacecraft are checked for every 16-second record, and the detector pointing vectors are computed only when the operational mode is explicitly determined. The attitude angles must be edited before they are used in computing the detector pointing vectors.

The measurement location calculations are made for both spacecraft using data directly from the spacecraft onboard attitude determination systems. The Attitude Determination and Control System (ADACS) on the NOAA spacecraft is a proven system. It has been flown and verified on several different spacecraft. The attitude angles are usually quite small, and normally their values do not exceed 0.1° during a 24-hour period. The ADACS for the ERBS spacecraft is a new system, however, and the angles derived directly from the onboard system are larger than those for the NOAA spacecraft. Comparisons of attitude data from the ERBS onboard attitude system with data generated by more refined ground-based calculations indicate that the onboard system is sufficiently accurate to meet ERBE measurement location requirements.

The local-horizon coordinate system in which the detector pointing vectors are calculated for the NOAA spacecraft by using the transformation matrix of equation (6) is identical to the common local-horizon system, in which all detector viewing vectors are finally determined. Thus, the detector pointing vectors for the NOAA spacecraft are given directly in the coordinate system of figure 3 as follows:

$$\begin{bmatrix} X_H \\ Y_H \\ Z_H \end{bmatrix} = \begin{bmatrix} X_{H,N} \\ Y_{H,N} \\ Z_{H,N} \end{bmatrix} \tag{7}$$

The transformation equation (5) determines the detector pointing vectors in one of two ERBS local-horizon systems. The orientations of these two coordinate systems, which differ when the ERBS spacecraft flies X-axis forward or X-axis rearward, are shown in relation to the common (NOAA) local-horizon coordinate system in figure 5. The ERBS spacecraft changes flight configurations by yawing (rotating about its Z-axis) 180° when the Sun is in the spacecraft orbit plane, which is the case approximately every 36 days. The transformations which determine the detector pointing vectors on the ERBS spacecraft in the common local-horizon coordinates are as follows:

For X-axis forward

$$\begin{bmatrix} X_H \\ Y_H \\ Z_H \end{bmatrix} = \begin{bmatrix} Z_{H,E} \\ -X_{H,E} \\ -Y_{H,E} \end{bmatrix} = \begin{bmatrix} 0 & 0 & 1 \\ -1 & 0 & 0 \\ 0 & -1 & 0 \end{bmatrix} \begin{bmatrix} X_{H,E} \\ Y_{H,E} \\ Z_{H,E} \end{bmatrix} \tag{8}$$

For X-axis rearward

$$\begin{bmatrix} X_H \\ Y_H \\ Z_H \end{bmatrix} = \begin{bmatrix} Z_{H,E} \\ X_{H,E} \\ Y_{H,E} \end{bmatrix} = \begin{bmatrix} 0 & 0 & 1 \\ 1 & 0 & 0 \\ 0 & 1 & 0 \end{bmatrix} \begin{bmatrix} X_{H,E} \\ Y_{H,E} \\ Z_{H,E} \end{bmatrix} \tag{9}$$

Orbit Ephemeris Data

The orbit ephemeris data for the ERBS and NOAA spacecraft are generated by GSFC. Tracking data for the ERBS spacecraft are obtained by the NASA Tracking and Data Relay Satellite and ground radar stations, and data for the NOAA spacecraft are provided by the U.S. Air Force North American Aerospace Defense Command. Eight days (one week with one overlap day) of ephemeris data are written on a single magnetic tape, which is shipped to LaRC weekly. Spacecraft position and velocity are contained on the ephemeris tape at 1-minute intervals, with the first data set for each day always at midnight universal time. Each 8-day ephemeris data set is processed through software at LaRC which evaluates the computed data for consistency and accuracy before the data are merged with the corresponding telemetry data and used to compute scanner measurement locations.

Measurement Location Computation in Earth Fixed Coordinates

In this second major step in determining the scanner Earth measurement locations, the unit pointing vector which describes the direction of the detector optical axis in the local-horizon coordinate system is transformed into an Earth fixed coordinate system. It is first necessary to transform all the pointing vectors and ephemeris data to the same coordinate system at the same time. This step is accomplished by merging instrument telemetry data and orbit position data as a function of time, interpolating the ephemeris data to the times of the scanner measurements, transforming pointing vectors and ephemeris states to the Earth fixed system, and finding the intersections of the pointing vectors with the Earth ellipsoid.

Interpolation of Ephemeris Data Times to Telemetry Data Times

As discussed previously, ephemeris state vectors are calculated at 60-second intervals, and telemetry data are recorded every 16 seconds. It is therefore necessary to interpolate the ephemeris data to the time of the telemetry records. This step is accomplished by converting two consecutive ephemeris state vectors to Keplerian orbit elements (ref. 2) and using these elements in linear interpolation to obtain orbit elements at the telemetry record times. These elements are then converted back to Cartesian state vectors to define the spacecraft position and velocity at the time of the telemetry record. Orbit element interpolation is justified because the Keplerian elements, except for true anomaly, change very slowly with time. True anomaly varies almost linearly with time in the near-circular orbits used by the ERBS and NOAA satellites.

Since scanner measurements are made at different times within a telemetry record, the spacecraft position must be further interpolated to the precise time of the measurement. The measurement time is obtained by adding the telemetry time offsets discussed previously to the universal time of the data record. Once the measurement times are known, the same linear interpolation scheme is used between telemetry record times to find the spacecraft state vector at each measurement time.

Coordinate Transformations

Inertial coordinates to Earth fixed coordinates. The ephemeris data are given in the inertial coordinate system (fig. 6) with the X_I-axis pointing toward the mean vernal equinox, the Z_I-axis coincident with the Earth's rotation axis, and the Y_I-axis forming a right-hand system.

The Earth fixed coordinate system has the X_F-axis at the Greenwich meridian, the Z_F-axis along the Earth's rotation axis, and the Y_F-axis forming a right-hand system. The matrix for the transformation from inertial to Earth fixed coordinates is

$$
\begin{bmatrix} X_F \\ Y_F \\ Z_F \end{bmatrix} = \begin{bmatrix} \cos\nu & \sin\nu & 0 \\ -\sin\nu & \cos\nu & 0 \\ 0 & 0 & 1 \end{bmatrix} \begin{bmatrix} X_I \\ Y_I \\ Z_I \end{bmatrix} \quad (10)
$$

where ν, the inertial longitude of Greenwich at the measurement time, is given in reference 2 by

$$
\nu = 99.6909833° + 36000.7689°T_u + 0.00038708°T_u^2 \\ + 360.9856463°\Delta T \quad (11)
$$

where

T_u = $(JD - 2\,415\,020)/36\,525$ = Julian centuries since 1900

JD = Julian date

ΔT = Fractional days between measurement time and midnight universal time

Local-horizon coordinates to Earth fixed coordinates. Pointing vectors for both spacecraft are given in the local-horizon system shown in figure 3. The transformation from the local-horizon system to the Earth fixed system (fig. 7) is done in two steps. The first step transforms the pointing vector from the local-horizon system to the local-geodetic system, which has X_G pointing north, Y_G pointing east, and Z_G pointing "down." The transformation matrix is

$$
\begin{bmatrix} X_G \\ Y_G \\ Z_G \end{bmatrix} = \begin{bmatrix} 0 & -\cos\eta & -\sin\eta \\ 0 & \sin\eta & -\cos\eta \\ 1 & 0 & 0 \end{bmatrix} \begin{bmatrix} X_H \\ Y_H \\ Z_H \end{bmatrix} \quad (12)
$$

where η, the heading angle, is the angle between north and the projection of the velocity vector in the tangent plane.

The second step of the transformation is from local-geodetic to Earth fixed coordinates as follows:

$$
\begin{bmatrix} X_F \\ Y_F \\ Z_F \end{bmatrix} = \begin{bmatrix} -\cos\Lambda\sin\Phi_G & -\sin\Lambda & -\cos\Lambda\Phi_G \\ -\sin\Lambda\sin\Phi_G & \cos\Lambda & -\sin\Lambda\cos\Phi_G \\ \cos\Phi_G & 0 & -\sin\Phi_G \end{bmatrix} \begin{bmatrix} X_G \\ Y_G \\ Z_G \end{bmatrix}
$$
$$(13)$$

where Λ is longitude and Φ_G is geodetic latitude. The relationship between geodetic and geocentric latitudes is found from the following equation (ref. 3):

$$\Phi_G = \tan^{-1}(\tan \Phi_C R_e^2/R_p^2) \tag{14}$$

where Φ_C is geocentric latitude, Φ_G is geodetic latitude, R_e is the equatorial radius of the Earth, and R_p is the polar radius.

The two transformations may be combined as follows to give the total transformation from local-horizon to Earth fixed coordinates:

$$\begin{bmatrix} X_F \\ Y_F \\ Z_F \end{bmatrix} = \begin{bmatrix} -\cos\Lambda\cos\phi_G & \cos\Lambda\sin\phi_G\cos\eta - \sin\Lambda\sin\eta & \cos\Lambda\sin\phi_G\sin\eta + \sin\Lambda\cos\eta \\ -\sin\Lambda\cos\phi_G & \sin\Lambda\sin\phi_G\cos\eta + \cos\Lambda\sin\eta & \sin\Lambda\sin\phi_G\sin\eta - \cos\Lambda\cos\eta \\ -\sin\phi_G & -\cos\phi_G\cos\eta & -\cos\phi_G\sin\eta \end{bmatrix} \begin{bmatrix} X_H \\ Y_H \\ Z_H \end{bmatrix} \tag{15}$$

Location Geometry at Top of Atmosphere

Once the spacecraft location and instrument pointing vectors are known in the Earth fixed coordinate system, the final step in locating the measurements is to find the intersection of the pointing vectors with the top of the Earth's atmosphere. The Earth is modelled by an ellipsoid with polar radius R_p and equatorial radius R_e. The height of the top of the atmosphere h is an arbitrary reference altitude (30 km) above the surface of the Earth and follows the equation

$$X^2/(R_e + h)^2 + Y^2/(R_e + h)^2 + Z^2/(R_p + h)^2 = 1 \tag{16}$$

Figure 8 illustrates the geometry of the pointing vector intersection. Given a vector pointing to the spacecraft $\overrightarrow{P}$ and a unit pointing vector $\widehat{V}$, the magnitude of the vector from the spacecraft to the intersection with the ellipsoid $\overrightarrow{V}$ is found from a root of the quadratic equation with the following coefficients:

$$\left.\begin{aligned} A &= (R_p + h)^2(\widehat{V}_x^2 + \widehat{V}_y^2) + (R_e + h)^2\widehat{V}_z^2 \\ B &= 2[(R_p + h)^2(P_x\widehat{V}_x + P_y\widehat{V}_y) + (R_e + h)^2 P_z\widehat{V}_z] \\ C &= (R_p + h)^2(P_x^2 + P_y^2) + (R_e + h)^2 P_z^2 \\ &\quad - (R_p + h)^2(R_e + h)^2 \end{aligned}\right\} \tag{17}$$

If $B^2 - 4AC < 0$, there is no intersection. One of the real roots is given by

$$|\overrightarrow{V}| = (-B - \sqrt{B^2 - 4AC})/2A$$

If this root is positive, it defines the magnitude of the vector from the spacecraft to the ellipsoid. If this root is negative, the pointing vector points away from the ellipsoid. The other root of the quadratic equation is the intersection of the pointing vector with the distant side of the ellipsoid.

The vector $\overrightarrow{R} = \overrightarrow{P} + \overrightarrow{V}$ is the vector from the center of the Earth to the intersection point shown in figure 8. Finally, the latitude and longitude of the Earth located measurement in Earth fixed geocentric coordinates are

$$\begin{aligned} \Phi_C &= \sin^{-1}(R_z/|\overrightarrow{R}|) \\ \Lambda_C &= \tan^{-1}(R_y/R_x) \end{aligned} \tag{18}$$

Method of Assessing Measurement Location Accuracy

The technique presented in the preceding section is used to calculate the location of all radiometric measurements. Some method is required to assess the accuracy of the technique. One way to compare the accuracy is to identify Earth features in the radiometric measurements. The shortwave radiometric measurements are not used because they include large variations due to clouds and are not useful at night. When there are large thermal contrasts, the longwave measurements show features such as a desert adjacent to an ocean. Using multiple scans across the thermal scene, the coastline between desert and ocean may be identified. This coastline may then be compared with an actual map, and errors in latitude and longitude or errors along and perpendicular to the subsatellite trace may be estimated. Coastline identification results for many days and several sites are accumulated on scatter plots, which allow biases in measurement locations to be detected.

9

Site-Selection Considerations and Restrictions

Four measurement sites have been chosen to satisfy the following conditions:

(a) Probable high thermal contrast between land and water. For example, at night during the summer, land is cooler than water, and during the day, land is warmer than water.

(b) Infrequent cloud cover. When clouds are present in a coastline scene, the longwave scanner measurements are much colder than either land or water. These measurements can be removed from the data set by using a minimum temperature cutoff.

(c) No unusual terrain features, such as lakes and mountains, next to the coastline. Lakes near the coastline have similar effects to those seen with ocean next to coastline, which makes discrimination difficult. Mountains may appear cold on one side and warm on the other side. This thermal contrast can be confused with that of land and water.

(d) Interesting coastline. An absolutely straight coastline would not be useful in detecting errors along the coastline. A coastline with regular curves, peninsulas, and bays is most useful.

In light of the preceding considerations, the following measurement sites have been chosen:

(a) Baja, California

(b) The northwest coast of Australia

(c) The coast of Libya

(d) The southeast coast of the Arabian peninsula

Some restrictions are applied to the data. Data values less than a threshold are presumed to be clouds and are not used. To avoid atmospheric effects such as limb darkening and refraction, data with scanner pointing angles greater than $30°$ measured from nadir are eliminated. To reduce extraneous thermal contrast due to inland terrain, data estimated to be more than 25 km from the coastline are not considered.

Finding a Scanner Coastline Crossing

The intersections of the pointing vectors with the TOA are extrapolated to the surface of the Earth (fig. 8), and these points on the surface are examined for coastline crossings. Figure 9 shows the plot of a typical longwave scan as it crosses a coastline. Each point represents one longwave scanner radiance measurement. Higher thermal measurements are presumed to be land in daytime and water at night.

Lower measurements are assumed to be the reverse. Thus, if there is a homogeneous land region bounded by water, a scan across the coastline boundary yields measurements similar to those shown in figure 9.

A cubic equation $y_i = ax_i^3 + bx_i^2 + cx_i + d$ ($i = 1, ..., 4$) is fitted to each set of 4 consecutive points for latitude and longitude. The inflection point for each equation $x = -b/3a$ is calculated for each set of 4 points. These inflection points are considered a coastal crossing if they fall between the two center points, x_2 and x_3, and if the change in the measurement

$$\Delta y = |y_1 - y_4|$$

is larger than a threshold value taken here to be 1 w/m^2/sr. A threshold value is used to eliminate spurious inflection points caused by normal variations in the measurements.

The coefficients of the cubic equation are found from

$$\begin{bmatrix} a \\ b \\ c \\ d \end{bmatrix} = \begin{bmatrix} x_1^3 & x_1^2 & x_1 & 1 \\ x_2^3 & x_2^2 & x_2 & 1 \\ x_3^3 & x_3^2 & x_3 & 1 \\ x_4^3 & x_4^2 & x_4 & 1 \end{bmatrix}^{-1} \begin{bmatrix} y_1 \\ y_2 \\ y_3 \\ y_4 \end{bmatrix} \tag{19}$$

Once a point has been selected as a coastal crossing, its location is determined by interpolating between the latitude and longitude of adjacent measurement locations.

Fitting a Collection of Coastal Crossings to a Map

Once a collection of coastal crossings has been calculated, it is fitted to a digitized map of the coastline of interest. It should be noted that the map coordinates are geodetic coordinates which differ in latitude from the calculated geocentric coordinates. This relationship between the two latitudes is given in equation (14).

Figures 10(a) through 10(d) show good examples of sets of crossings plotted on maps. The circles represent the calculated coastline crossings, and the squares are the subsatellite points. Most sets of crossings do not produce useful information because of the presence of clouds or poor thermal contrast at the time of satellite passage.

Some figure of merit is needed to determine how well the estimated coastline matches the map coastline. The figure of merit chosen is the least-squares distance between the calculated coastal crossings and the map coordinates of the coastline. A latitude and

longitude correction is applied to each member of the set of crossings in a manner which minimizes the sum of the squares of the distances from the crossings to the map. This correction is then defined as the location error for the satellite pass.

Along-Track and Cross-Track Errors

Since much of the error in locating measurements may be attributed to spacecraft attitude errors and errors in the adjustment to detector elevation angle, it is useful to consider the measurement location errors in a coordinate system which is aligned with the scan direction. The mapping from latitude and longitude coordinates to along-track and cross-track coordinates is shown in figure 11 and is given by

$$\begin{bmatrix} \epsilon_c \\ \epsilon_a \end{bmatrix} = \begin{bmatrix} \pm \sin \eta & \cos \eta \\ -\cos \eta & \pm \sin \eta \end{bmatrix} \begin{bmatrix} \epsilon_\Lambda \\ \epsilon_\Phi \end{bmatrix} \quad (20)$$

where η is spacecraft heading angle, ϵ_c is cross-track error, ϵ_a is along-track error, ϵ_Λ is longitude error, and ϵ_Φ is latitude error. The upper sign $(+)$ in equation (20) is used when the scan direction is left to right; otherwise, the lower sign $(-)$ is used. The latitude effect on longitude error is ignored, because the sites considered are near the equator. For example, figure 10(a) shows that the least-squares latitude and longitude errors map into errors of $-0.0478°$ cross track and $0.0271°$ along track.

Statistical Treatment of Results

The along-track and cross-track errors from different sites and different days may be used to determine biases in the location of the measurements. Figure 12 shows a scatter plot of data from the ERBS satellite for November 1984. Each point on the plot is the result of analyzing the coastline crossings for a single site. The solid ellipse is the 95-percent probability ellipse computed assuming that the data have a Gaussian distribution with mean and covariance equal to that of the data. The center of the ellipse identifies a bias along each axis. Figure 12 shows a cross-track bias of $-0.026°$ (about 2.9 km) and an along-track bias of $0.0048°$ (about 0.53 km). The variance implied by the probability ellipse is an underestimate, because scan angles are limited to those within $30°$ of nadir. For a given pointing error, the error in Earth location increases with scan angle as measured from nadir.

Results and Discussion

The method for calculating ERBE scanner measurement locations presented here has been implemented in the operational data processing system.

Every scanner measurement is located by using the full set of transformations and interpolations. These results are based upon operational flight data.

The coastline detection method has been applied to many days of data for both the ERBS and NOAA 9 satellites. Figures 10(a) through 10(d) illustrate orbital passes over Baja, California, the northwestern coast of Australia, the Gulf of Sidra off Libya, and the southeast coast of the Arabian peninsula. The square symbols show the subsatellite track during the pass; the detected coastline crossings for each scan are drawn as circles. The estimated coastlines appear to follow the map quite well. In figure 10(a), one point in the northeast portion of the Gulf of California appears to be 20 to 30 km from the coast. In fact, there is an island, Isla del Tiburon, which is not digitized on the map but is detected by the scanner.

Individual scanner measurements in figure 10(a) show a difference of up to 15 km between the estimated coastline crossing and the actual mapped coastline. When the coastline fitting technique is used, the average error for all crossings during the pass is 6.1 km. This error may be apportioned between $0.027°$ along-track error and $-0.048°$ cross-track error. These errors are approximately 3 and 5 km, respectively.

The location error for a single satellite pass over a coastline may not be representative of the operation of the satellite over all orbital conditions. Therefore, additional passes must be investigated. A scatter diagram of along-track and cross-track errors for all coastline crossings identified for the ERBS satellite during November 1984 is presented in figure 12. Each point in this diagram represents the average error for a single map of one of the coastal areas. For example, the results for figure 10(a) are collapsed to a single point in this plot. A small but persistent cross-track bias is illustrated by the 95-percent confidence ellipse which is centered about $-0.03°$ in the cross-track direction. This direction is opposite to the direction of scan motion during this time period. The bias represents a 3-km location error. To correct for this bias, the instrument response time adjustment to the effective scan elevation angle has been reduced from $3.066°$ to $2.85°$.

Figure 13 shows results for the northwest coast of Australia. Figure 13(a) uses a response time adjustment of $3.066°$, and figure 13(b) uses an adjustment of $2.85°$. A comparison of the figures shows that the estimated coastline is closer to the map coastline for the reduced instrument response time adjustment. The corrected time adjustment is used in the operational processing system.

11

As discussed previously, the ERBS Attitude Determination and Control System is new, and the attitude angles derived from the onboard system are larger than those for the NOAA spacecraft. Ground-based processing of ERBS ADACS data has been performed at GSFC to produce more accurate (definitive) attitude data for selected periods. The coastline detection results for ERBS shown in figure 14 illustrate scanner measurement locations based on a set of these definitive attitude data. The results shown are for the same geographical area and time period as those of figure 10(d), but the scanner measurement locations in figure 10(d) are based on attitude data derived from the onboard attitude determination system. This comparison is typical, and the very close agreement between the two sets of coastline detection results indicates that the attitude data from the ERBS onboard determination system is sufficiently accurate for ERBE measurement location calculations.

Figure 15 presents April 1985 results for both the ERBS and NOAA 9 satellites. Again, the diagram plots along-track location errors versus cross-track location errors by using the average error during a satellite pass. These errors include the bias correction to the response-time adjustment for both satellites. The error ellipsoids show that 95 percent of all coastline detections fall within approximately 10 km of the true coastline location. The mean and standard deviation along each axis of these scatter diagrams are shown in the following table:

	Cross track		Along track	
Satellite	Mean, km	Standard deviation, km	Mean, km	Standard deviation, km
ERBS	0.09	4.61	0.49	3.67
NOAA 9	−.39	4.88	−1.17	3.43

The average errors are much smaller than the scanner field of view, which is about 40 km. Also, the scatter of points as measured by the standard deviation along each axis is consistent between satellites. This consistency shows that error sources contributing to the measurement location errors are similar for ERBS and NOAA 9.

Conclusions

Based upon the results from the coastline detection technique developed here, the accuracy of the Earth Radiation Budget Experiment (ERBE) scanner measurement location appears to be well within the limits of the detector field of view. Results of this study indicate the following conclusions:

1. Satellite ephemeris data are accurate and are merged properly with telemetry data for both the Earth Radiation Budget Satellite (ERBS) and the NOAA 9 satellite.

2. The ERBS onboard attitude determination system produces attitude angle data which are sufficiently accurate for ERBS scanner location calculations.

3. At pointing angles within 30° of nadir, single estimates of a coastline location from the scanner radiometric data are less than 15 km in error.

4. An average of all coastline detections from a single satellite pass is less than 10 km in error.

5. For both the ERBS and NOAA 9 satellites, all passes of April 1985 have an average location error of less than 1.2 km, and the standard deviation of the error is less than 5 km in both the along-track and cross-track directions.

Users of the ERBE data may rely upon the geographic location as identified on the archival products. However, it should be noted that the geocentric coordinates identified in the ERBE data-tape products must be transformed to geodetic map coordinates before making comparisons. The ERBE project intends to monitor the measurement location accuracy by using the coastline detection technique for the life of the instruments.

References

1. Barkstrom, Bruce R.: The Earth Radiation Budget Experiment (ERBE). *American Meteorol. Soc. Bull.*, vol. 65, no. 11, 1984, pp. 1170–1185.

2. Escobal, Pedro Ramon: *Methods of Orbit Determination.* John Wiley & Sons, Inc., c.1965.

3. Melbourne, William G.; Mulholland, J. Derral; Sjogren, William L.; and Sturms, Francis M., Jr.: *Constants and Related Information for Astrodynamic Calculations, 1968.* Tech. Rep. No. 32-1306 (Contract NAS7-100), Jet Propulsion Lab., California Inst. of Technology, July 15, 1968. (Available as NASA CR-97666.)
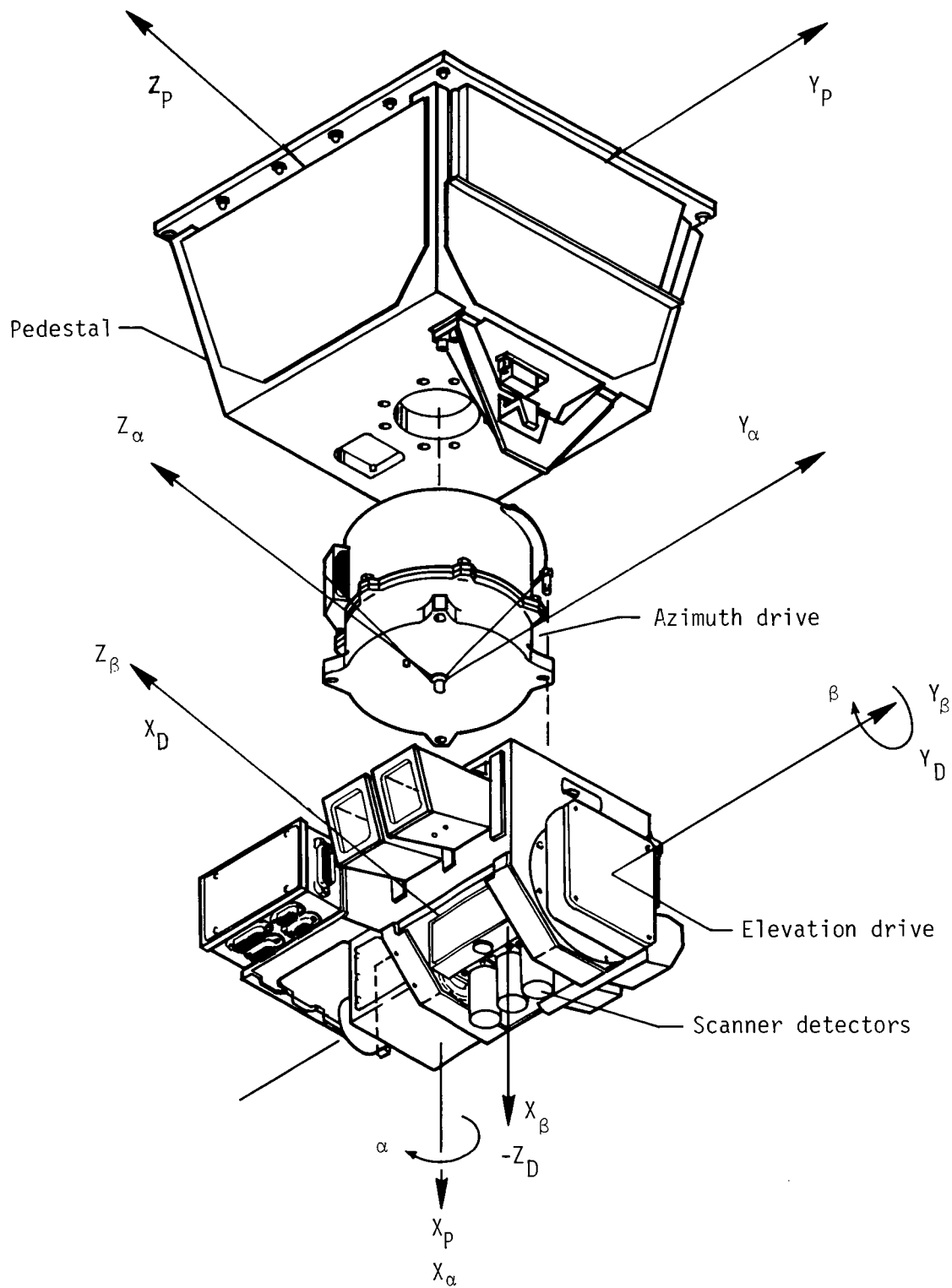
Figure 1. Coordinate systems of ERBE scanner instrument.
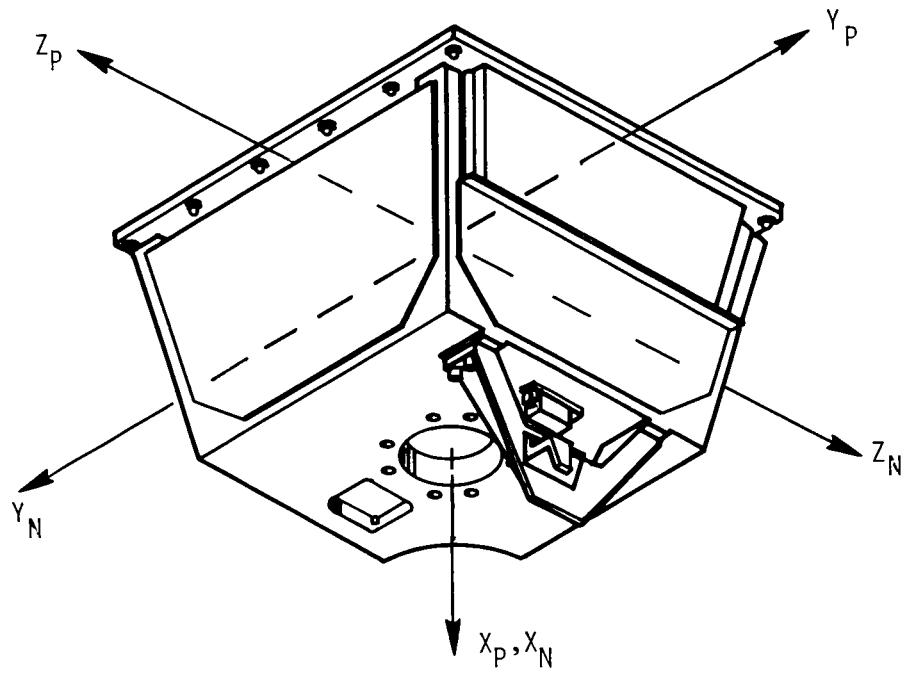
(a) NOAA.
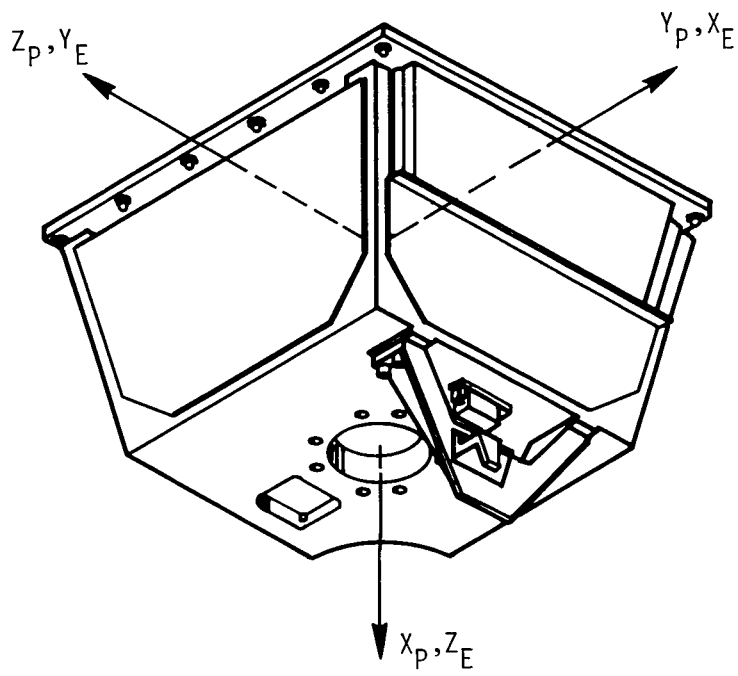
(b) ERBS.

Figure 2. Relationship between instrument pedestal and spacecraft coordinate systems.
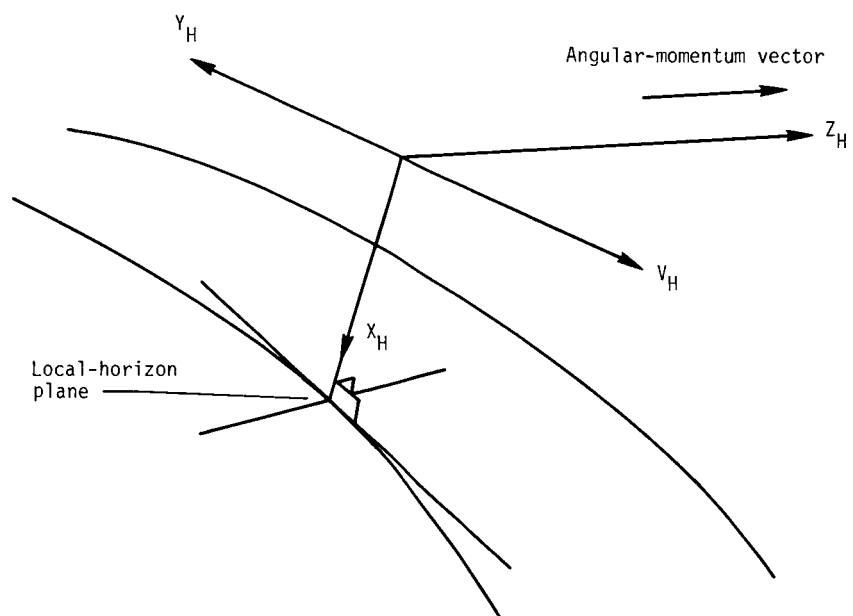
Figure 3. Final local-horizon coordinate system for computing pointing vectors.
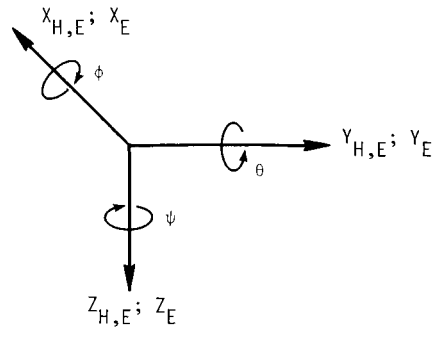
(a) ERBS.
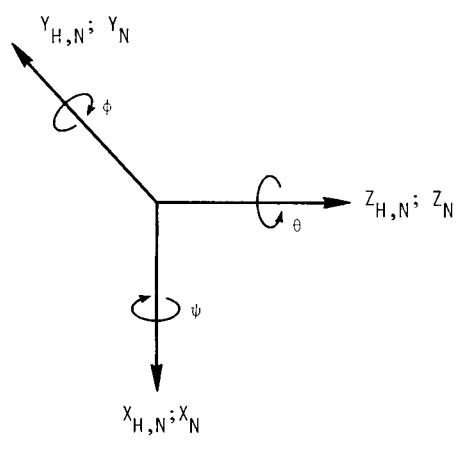
(b) NOAA.

Figure 4. Relationship between a spacecraft coordinate system and corresponding local-horizon coordinate system.
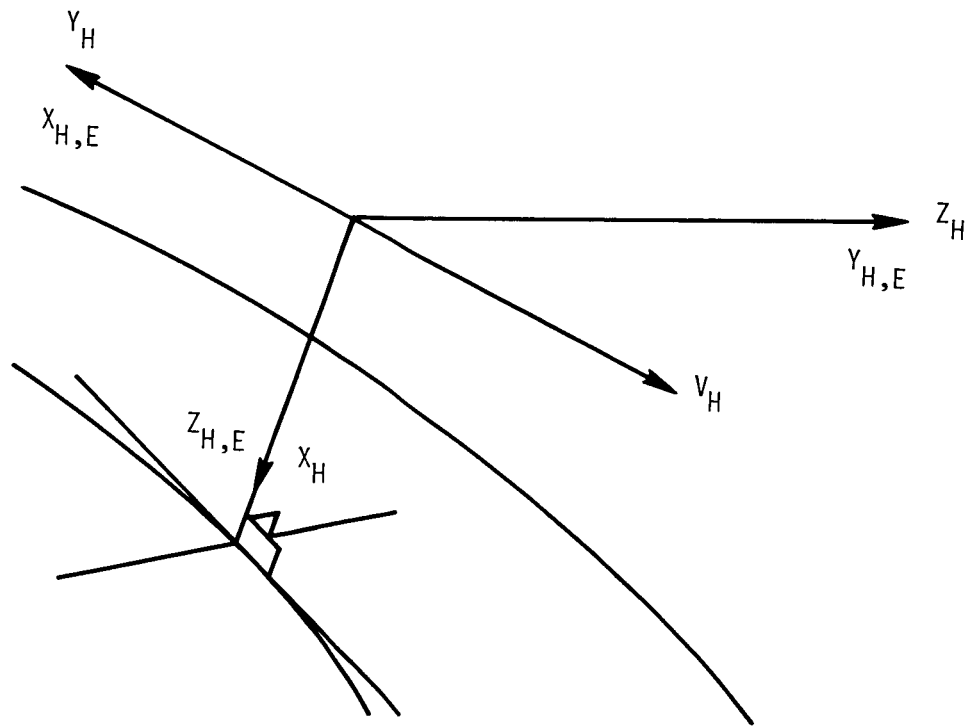
(a) ERBS with X-axis rearward.
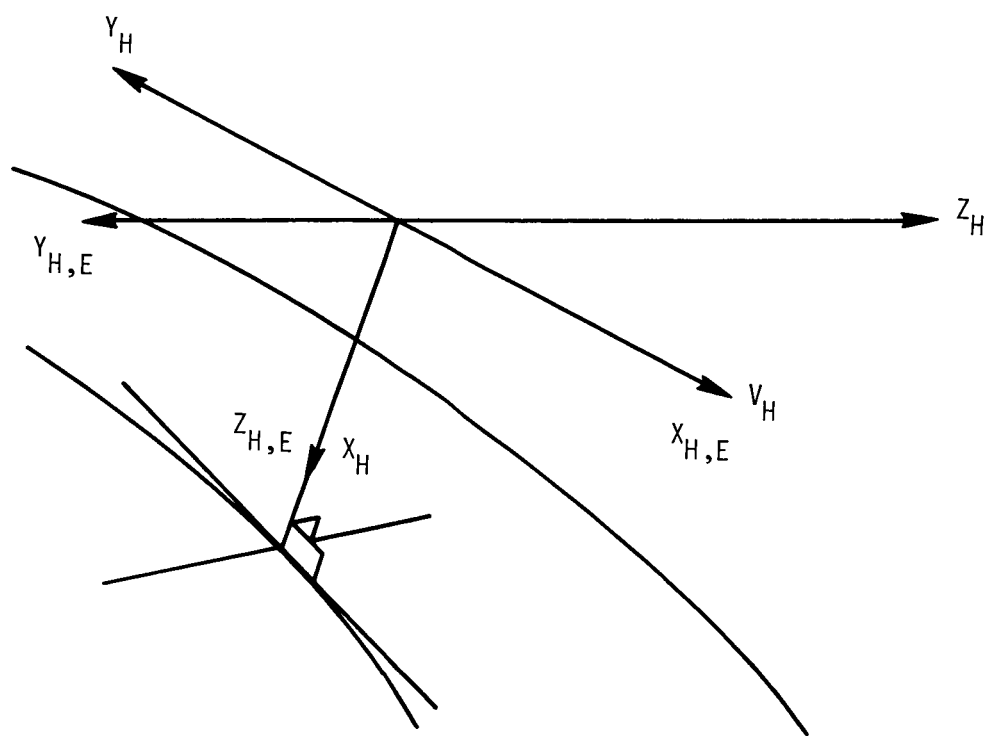
(b) ERBS with X-axis forward.

Figure 5. Relationship between ERBS local-horizon coordinate systems and final local-horizon system.
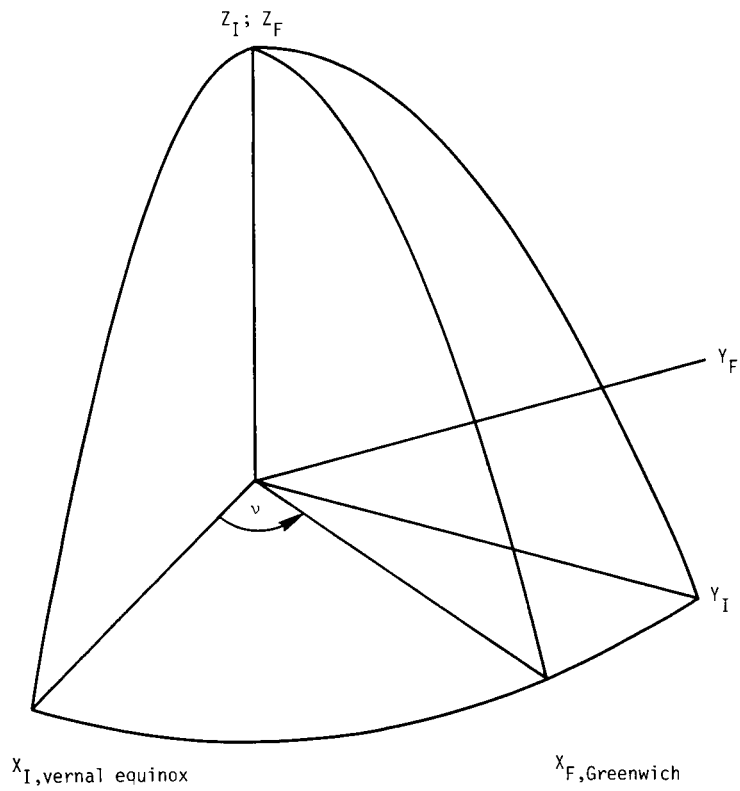
Figure 6. Geometry of transformation from inertial to Earth fixed coordinates.
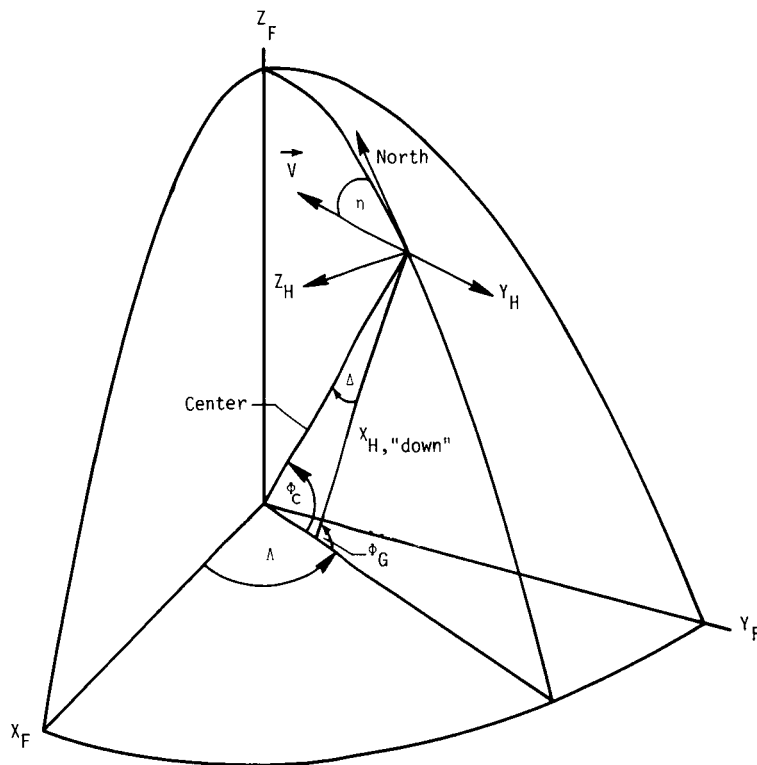
Figure 7. Geometry of transformation from local-horizon to Earth fixed coordinates.
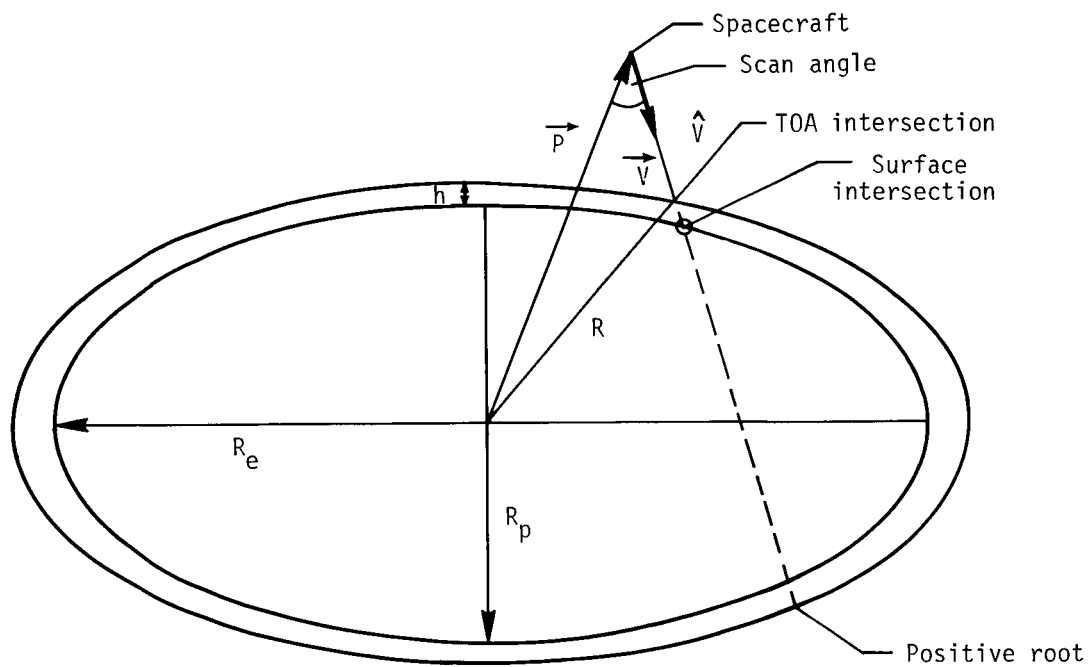
Figure 8. Intersection of pointing vector with Earth ellipsoid.
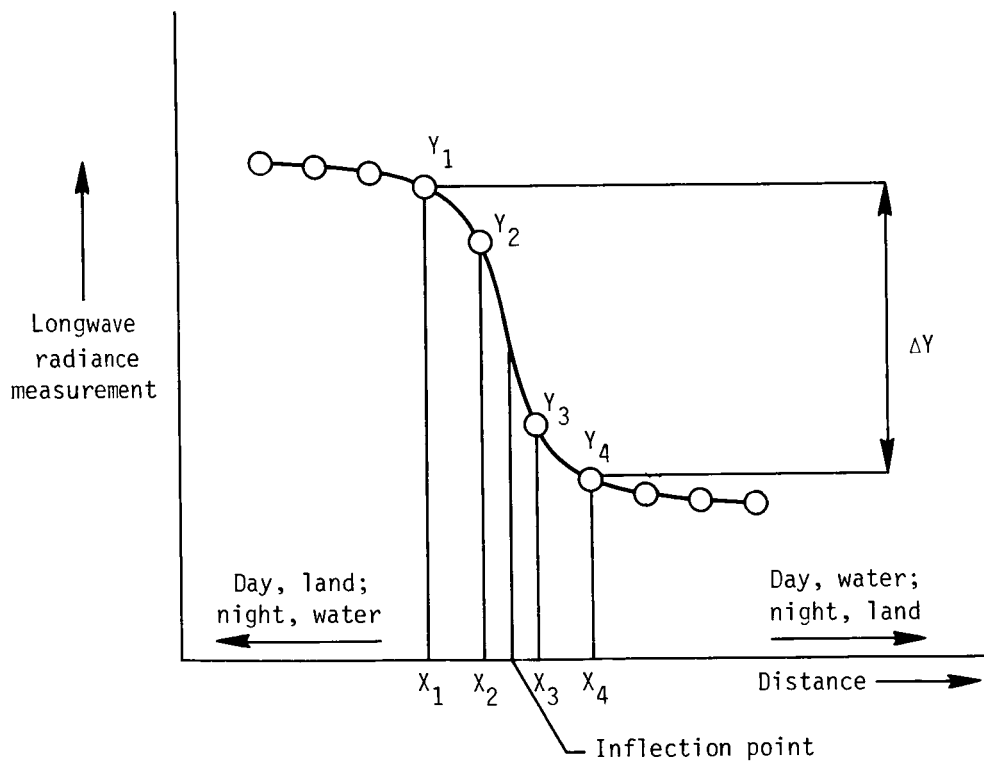
Figure 9. Cubic fit for coastline detection.
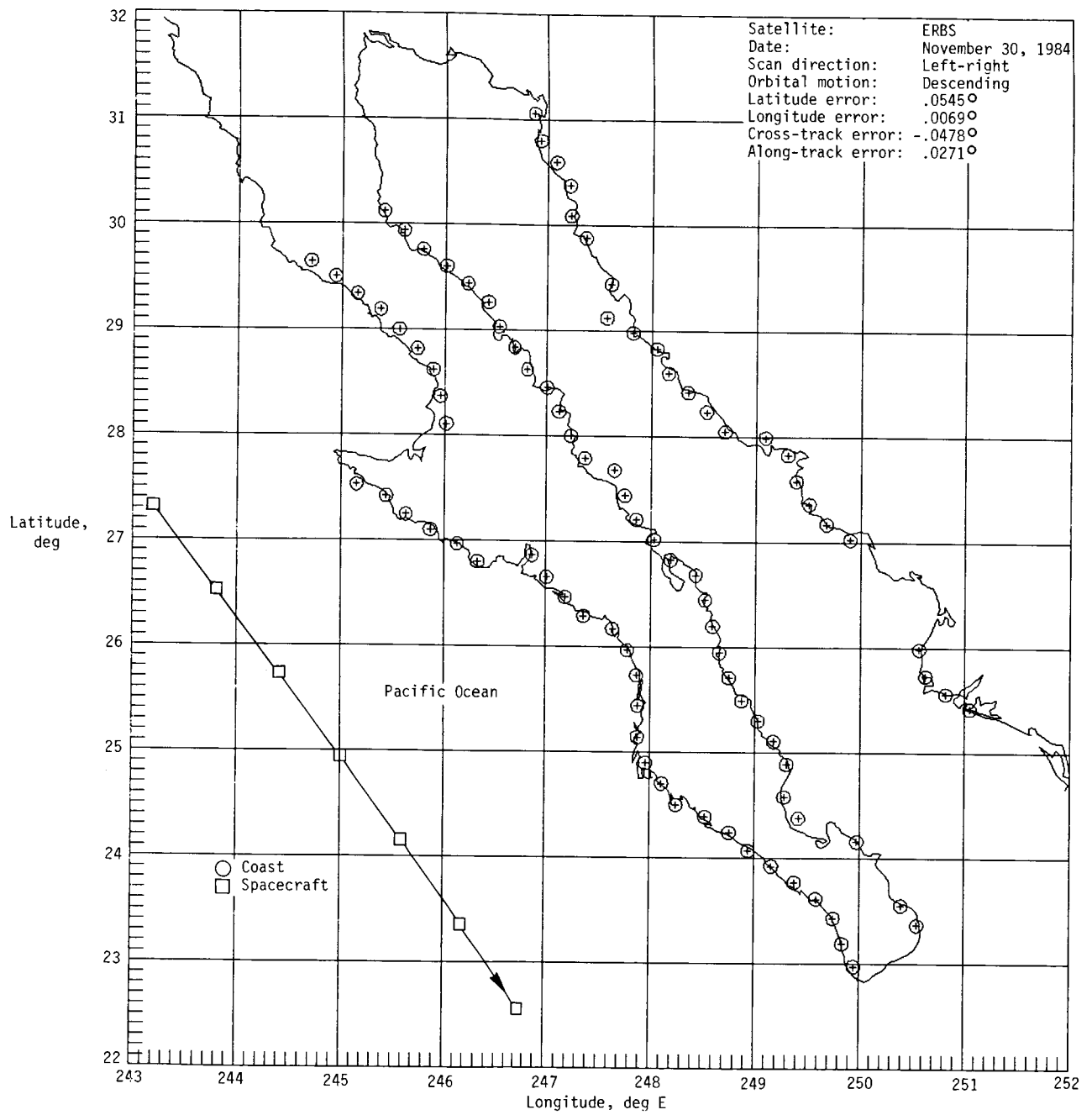
(a) Baja, California.

Figure 10. Coastline detection results.
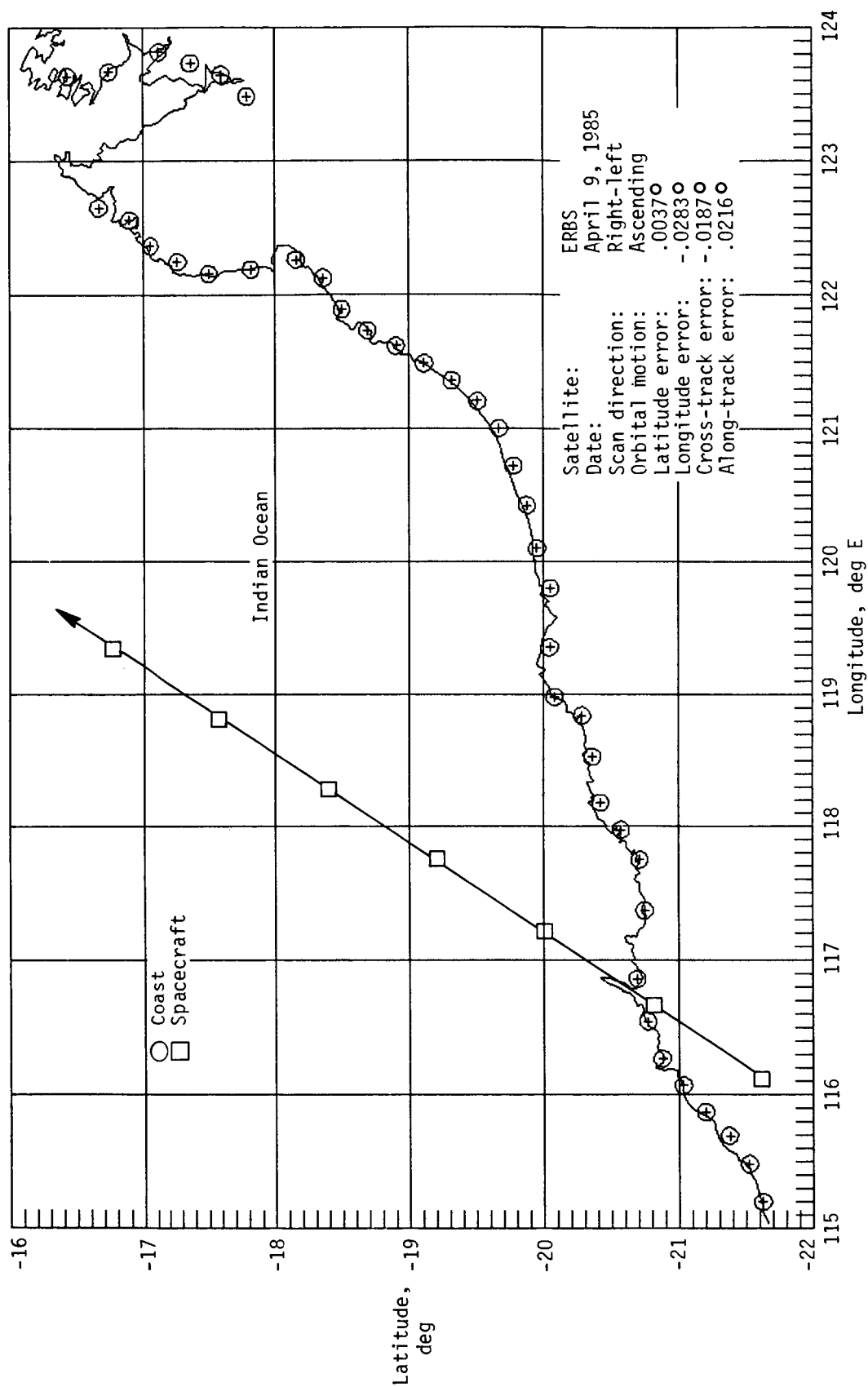
(b) Australia.

Figure 10. Continued.

Satellite: NOAA
Date: April 9, 1985
Scan direction: Right-left
Orbital motion: Ascending
Latitude error: -.0308○
Longitude error: .0151○
Cross-track error: .0253○
Along-track error: -.0231○

Mediterranean Sea

○ Coast
□ Spacecraft
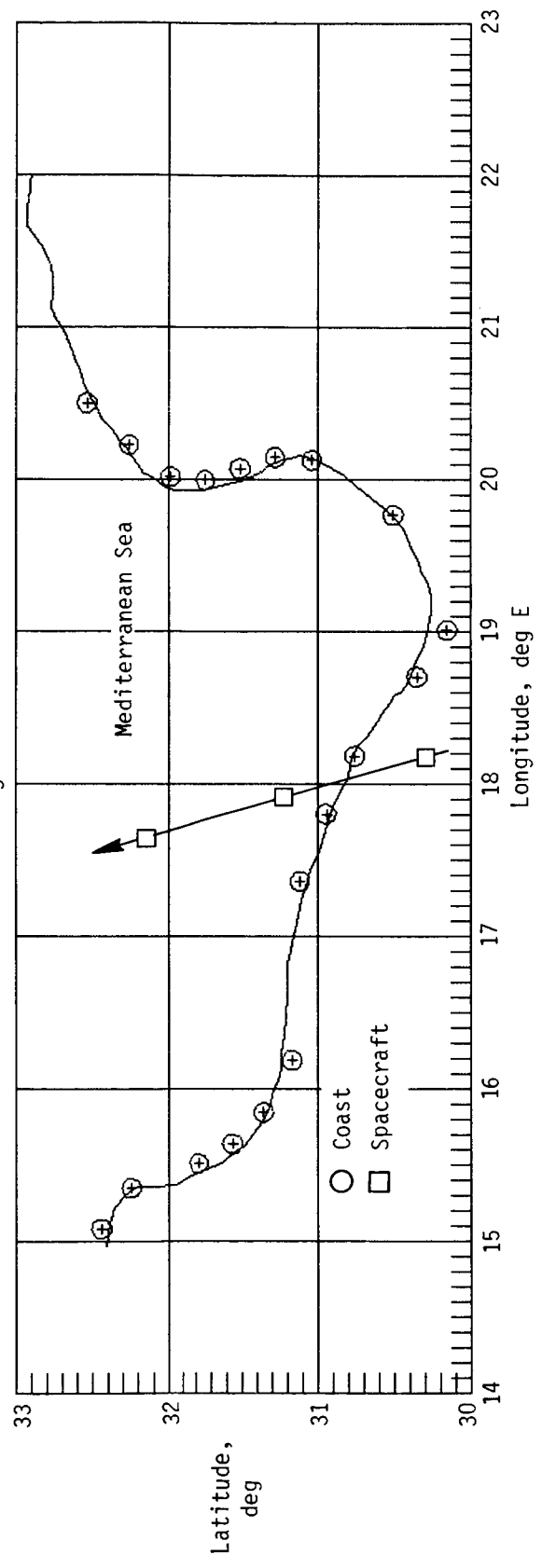
Latitude, deg E

(c) Libya.

Figure 10. Continued.
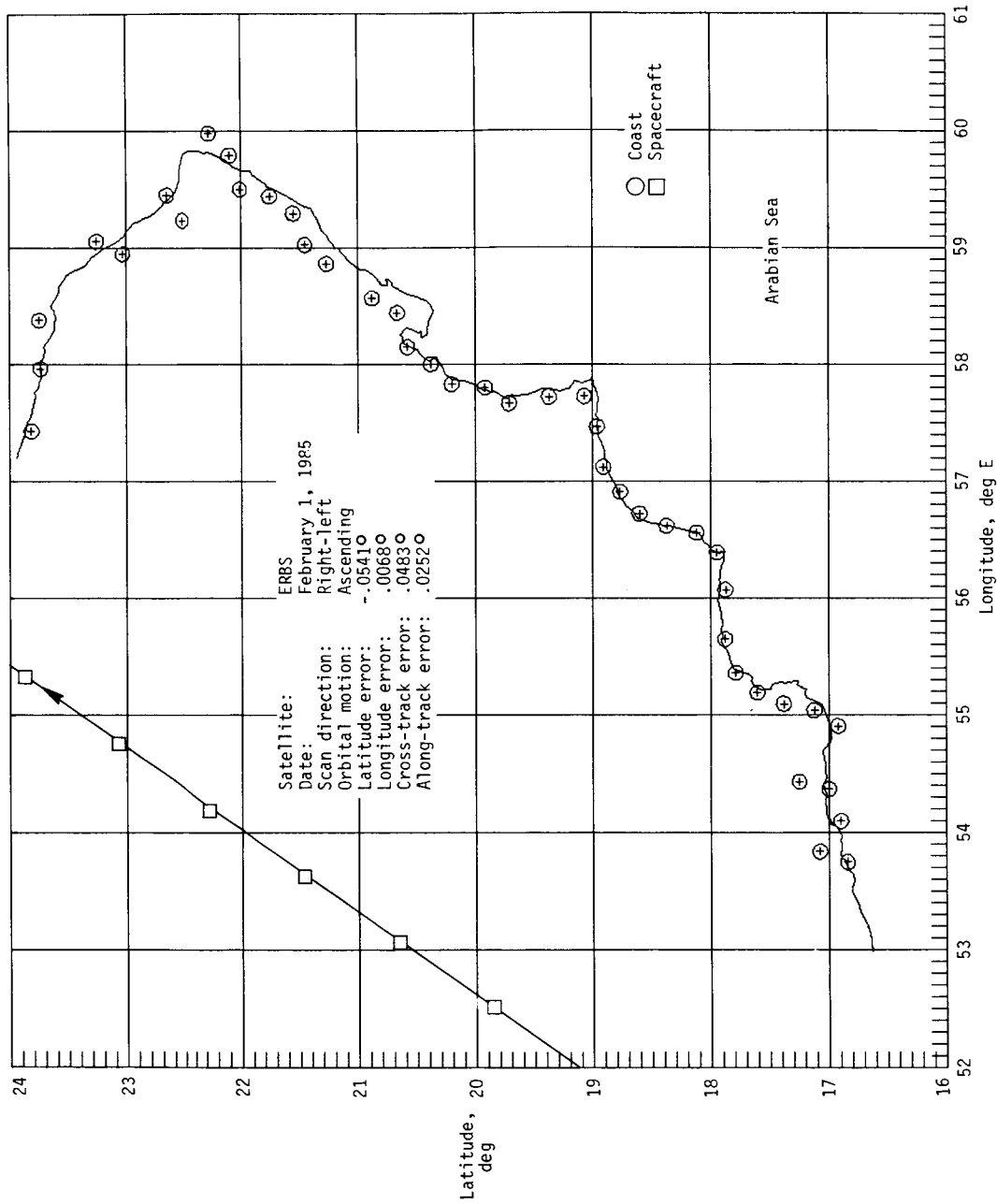
(d) Arabian peninsula.

Figure 10. Concluded.
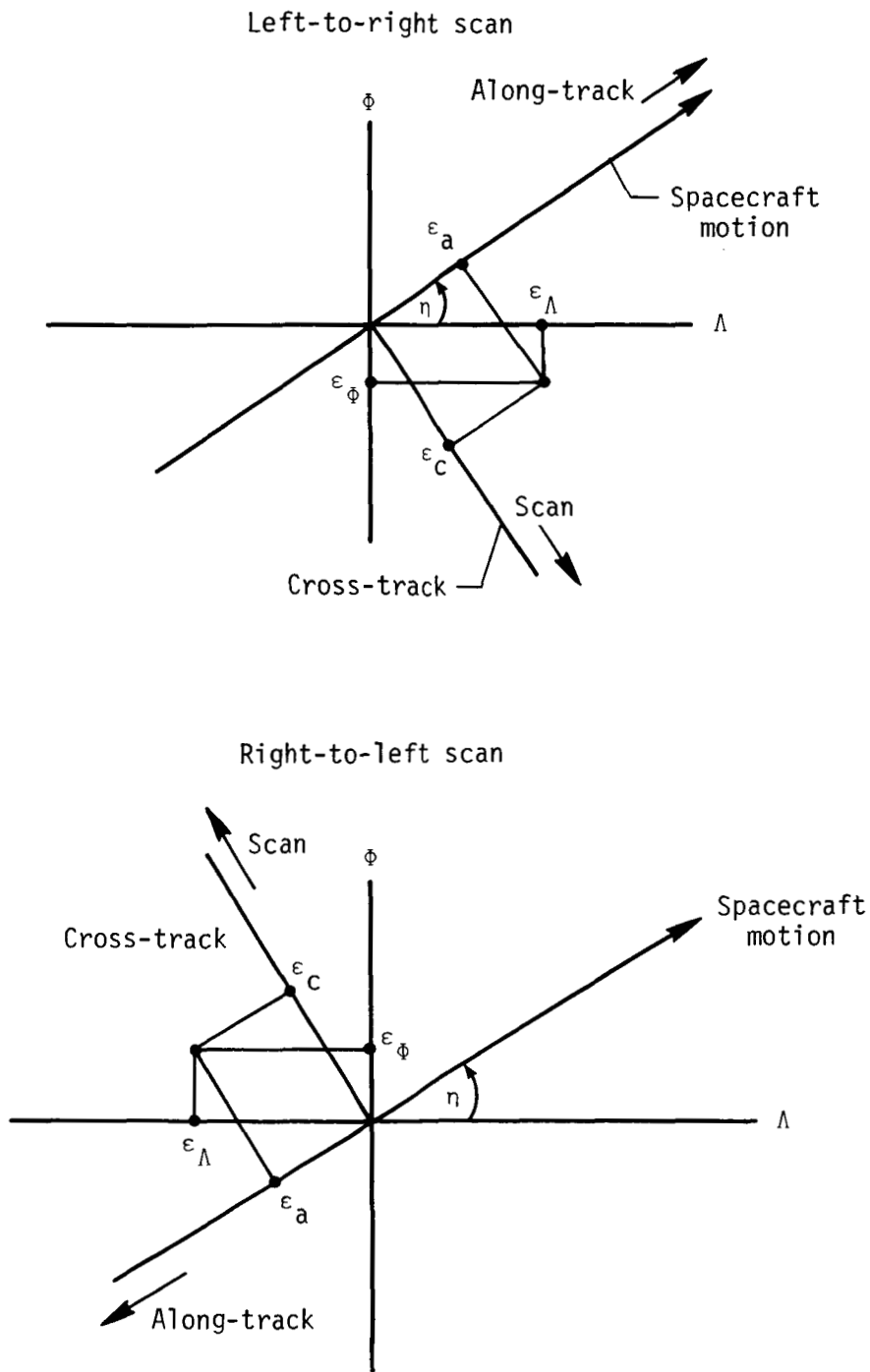
Figure 11. Geometry of transformations from latitude and longitude to along-track and cross-track coordinates.
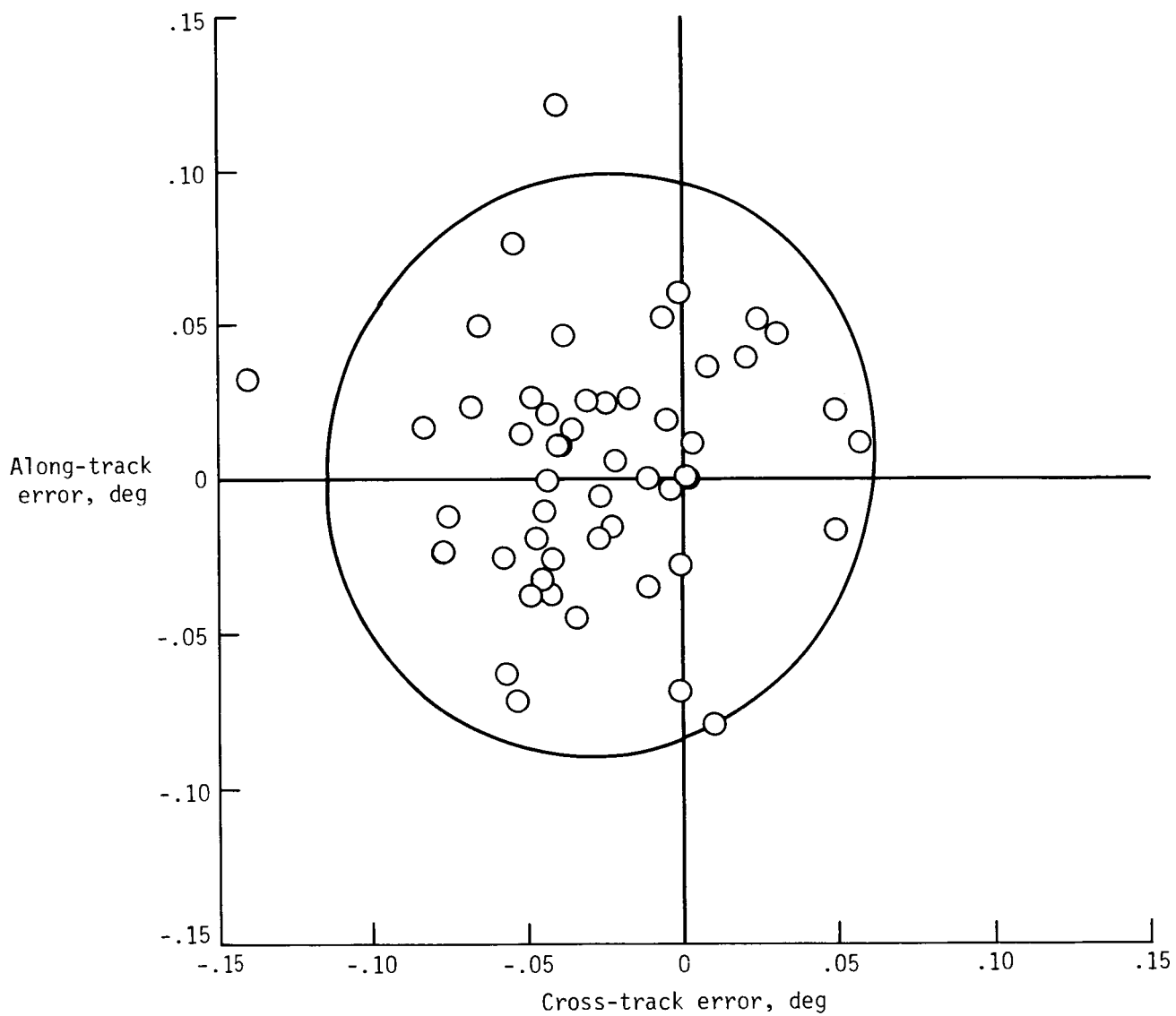
Figure 12. Preliminary ensemble location errors for ERBS satellite in November 1984.

Satellite: ERBS
Date: November 9, 1984
Scan direction: Right-left
Orbital motion: Ascending
Latitude error: .0019 O
Longitude error: -.0937 O
Cross-track error: -.0535 O
Along-track error: .0770 O

Indian Ocean

O Coast
□ Spacecraft

Latitude, deg

Longitude, deg E
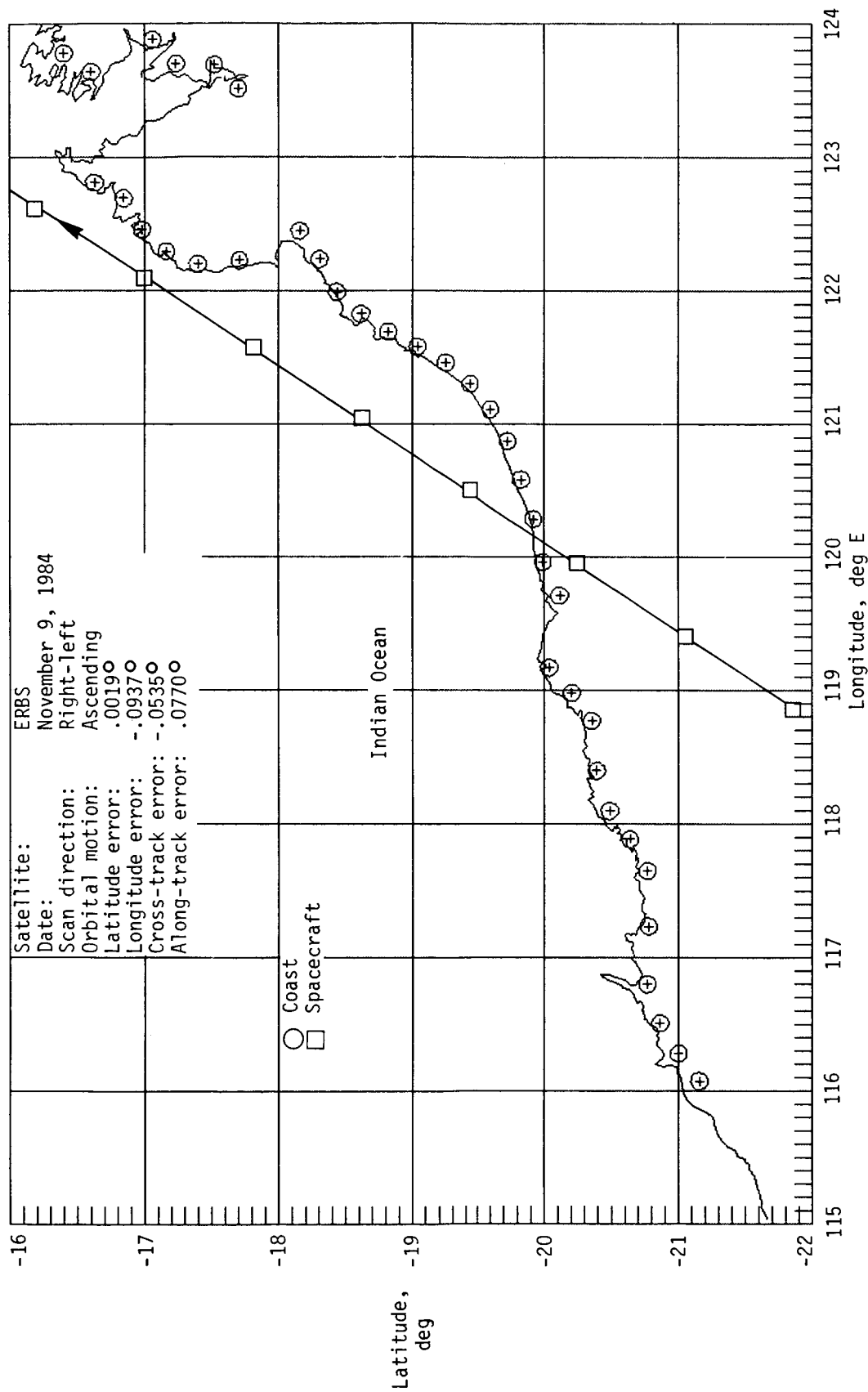
(a) 3.066°.

Figure 13. Effect of instrument response time adjustment to effective scan elevation angle for Australian site.

Satellite: ERBS
Date: November 9, 1984
Scan direction: Right-left
Orbital motion: Ascending
Latitude error: -.0092 ○
Longitude error: -.0831 ○
Cross-track error: -.0383 ○
Along-track error: .0743 ○

Indian Ocean

○ Coast
□ Spacecraft

Longitude, deg E

Latitude, deg
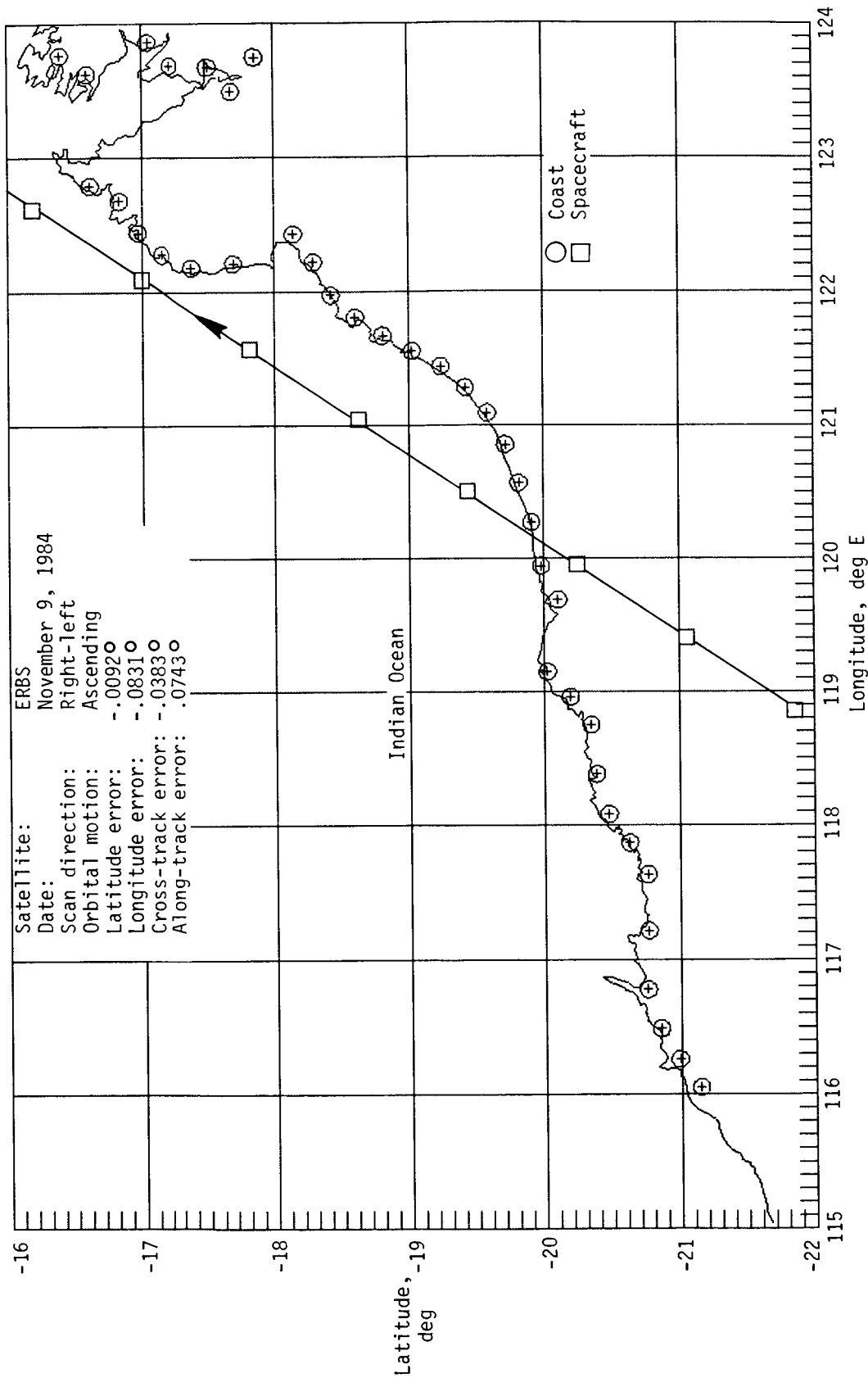
(b) 2.85°.

Figure 13. Concluded.
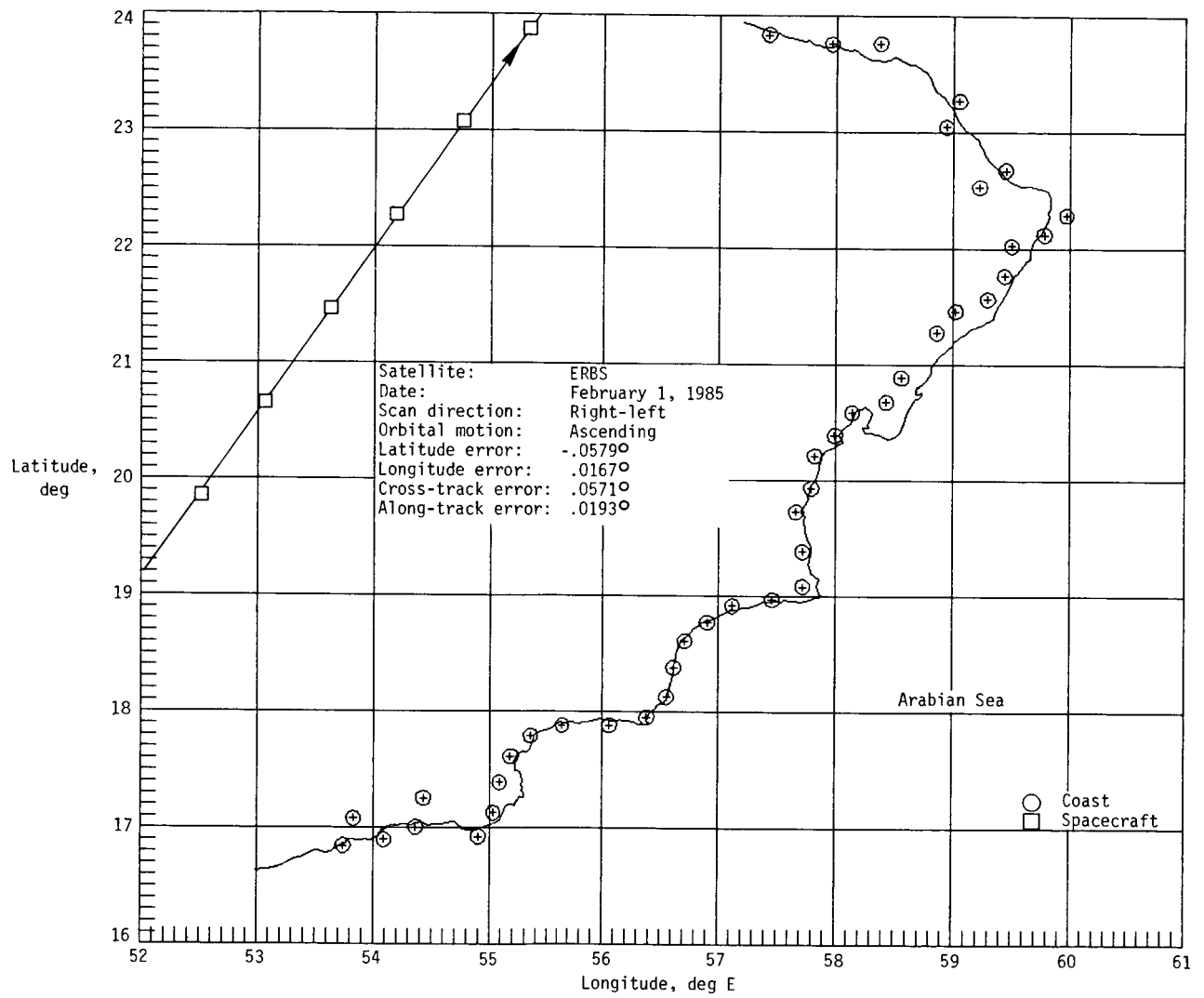
Figure 14. Effect of using definitive attitude data for Arabian site.
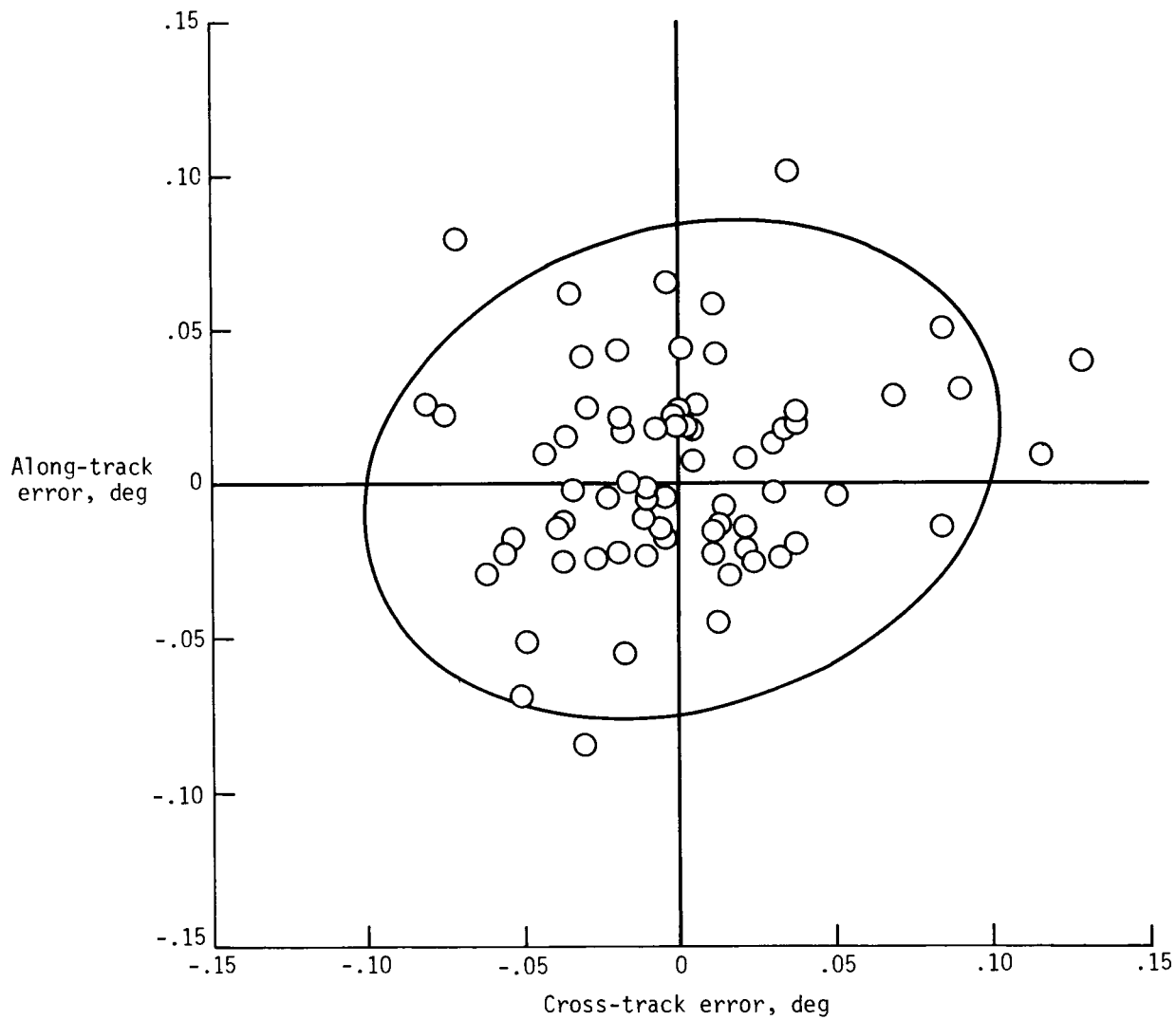
(a) ERBS.

Figure 15. Ensemble location errors for April 1985.
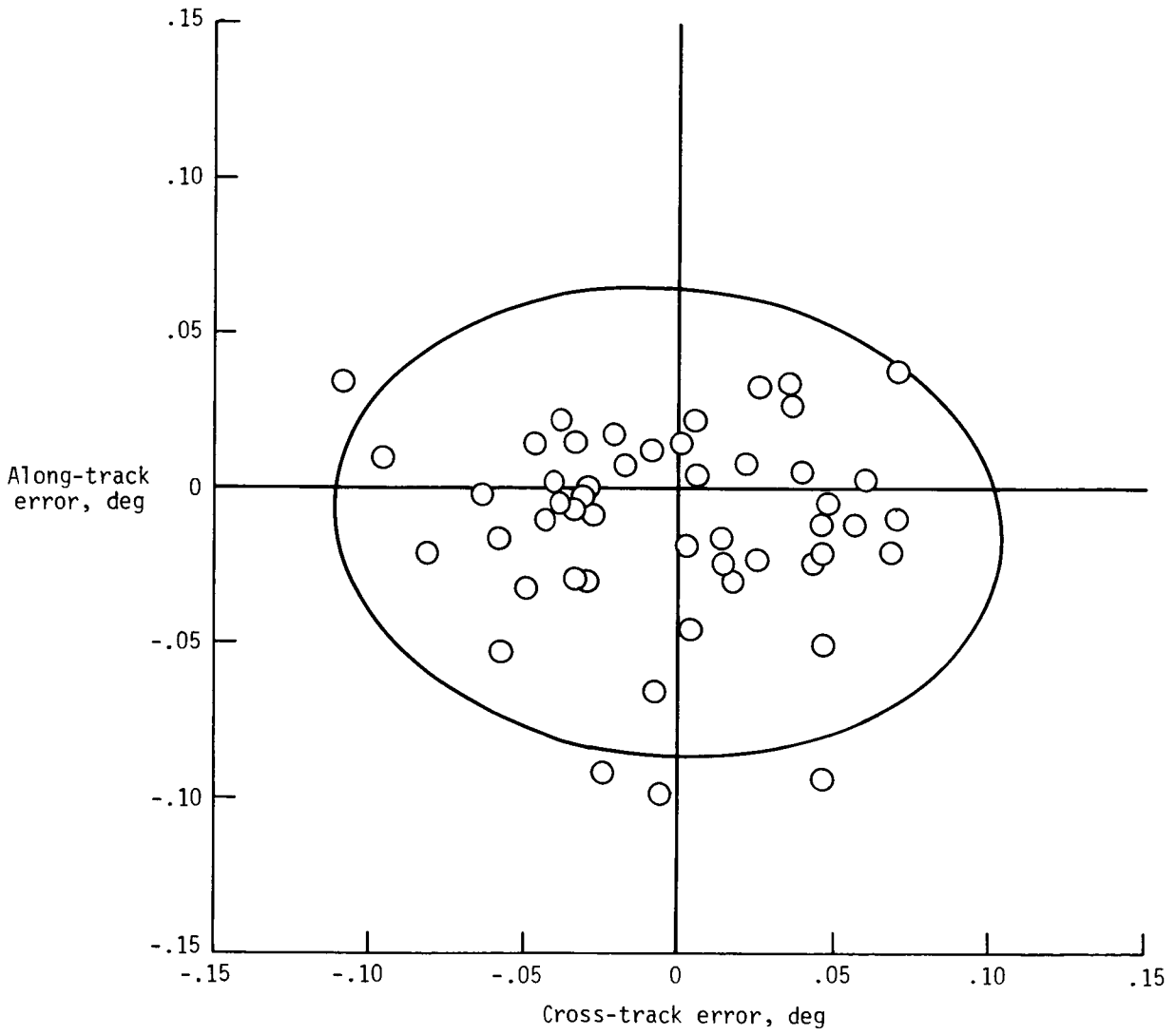
(b) NOAA 9.

Figure 15. Concluded.

Report Documentation Page

1. Report No. NASA TP-2670	2. Government Accession No.	3. Recipient's Catalog No.
4. Title and Subtitle Calculation and Accuracy of ERBE Scanner Measurement Locations		5. Report Date September 1987
		6. Performing Organization Code
7. Author(s) Lawrence H. Hoffman, William L. Weaver, and James F. Kibler		8. Performing Organization Report No. L-16218
9. Performing Organization Name and Address NASA Langley Research Center Hampton, VA 23665-5225		10. Work Unit No. 665-45-20-01
		11. Contract or Grant No.
12. Sponsoring Agency Name and Address National Aeronautics and Space Administration Washington, DC 20546-0001		13. Type of Report and Period Covered Technical Paper
		14. Sponsoring Agency Code
15. Supplementary Notes		

16. Abstract

The Earth Radiation Budget Experiment (ERBE) uses scanning radiometers to measure shortwave and longwave components of the Earth's radiation field at about 40 km resolution. It is essential that these measurements be accurately located at the top of the Earth's atmosphere so they can be properly interpreted by users of the data. Before the launch of the ERBE instrument sets, a substantial emphasis was placed on understanding all factors which influence the determination of measurement locations and properly modelling those factors in the data processing system. After the launch of ERBE instruments on the Earth Radiation Budget Satellite and NOAA 9 spacecraft in 1984, a coastline detection method was developed to assess the accuracy of the algorithms and data used in the location calculations. Using inflight scanner data and the coastline detection technique, the measurement location errors are found to be smaller than the resolution of the scanner instruments. This accuracy is well within the required location knowledge for useful science analyses.

17. Key Words (Suggested by Authors(s)) ERBE Remote sensing	18. Distribution Statement Unclassified—Unlimited Subject Category 88	
19. Security Classif.(of this report) Unclassified	20. Security Classif.(of this page) Unclassified	21. No. of Pages 32	22. Price A03